Adaptive Subpixel Mapping Based on a Multiagent System for Remote-Sensing Imagery

Xiong Xu, Yanfei Zhong, *Member, IEEE*, and Liangpei Zhang, *Senior Member, IEEE*

***Abstract*— The existence of mixed pixels is a major problem in remote-sensing image classification. Although the soft classification and spectral unmixing techniques can obtain an abundance of different classes in a pixel to solve the mixed pixel problem, the subpixel spatial attribution of the pixel will still be unknown. The subpixel mapping technique can effectively solve this problem by providing a fine-resolution map of class labels from coarser spectrally unmixed fraction images. However, most traditional subpixel mapping algorithms treat all mixed pixels as an identical type, either boundary-mixed pixel or linear subpixel, leading to incomplete and inaccurate results. To improve the subpixel mapping accuracy, this paper proposes an adaptive subpixel mapping framework based on a multiagent system for remote-sensing imagery. In the proposed multiagent subpixel mapping framework, three kinds of agents, namely, feature detection agents, subpixel mapping agents and decision agents, are designed to solve the subpixel mapping problem. Experiments with artificial images and synthetic remote-sensing images were performed to evaluate the performance of the proposed subpixel mapping algorithm in comparison with the hard classification method and other subpixel mapping algorithms: subpixel mapping based on a back-propagation neural network and the spatial attraction model. The experimental results indicate that the proposed algorithm outperforms the other two subpixel mapping algorithms in reconstructing the different structures in mixed pixels.**

***Index Terms*— Multiagent system, remote sensing, resolution enhancement, subpixel mapping, super-resolution mapping.**

I. Introduction

REMOTE sensing has become an important source of land use/cover information at a range of spatial and temporal scales [1]. Traditional classification techniques assign every pixel to a single class, but remote-sensing images, particularly at coarse spatial resolutions, are commonly dominated by mixed pixels that contain more than one class on the ground [2]. To obtain the subpixel information, soft classification techniques and spectral unmixing algorithms have been used to obtain the fraction of each class in a pixel [3]–[5]. However, the subpixel spatial attribution of the different classes in a pixel will still be unknown with these techniques.

Manuscript received November 11, 2011; revised December 27, 2012; accepted January 20, 2013. Date of publication March 13, 2013; date of current version December 12, 2013. This work was supported in part by the National Basic Research Program of China (973 Program) under Grant 2011CB707105, in part by the National Natural Science Foundation of China under Grant 40901213, and in part by the Foundation for the Author of National Excellent Doctoral Dissertation of P.R. China (FANEDD) under Grant 201052.

The authors are with the State Key Laboratory of Information Engineering in Surveying, Mapping and Remote Sensing, Wuhan University, Wuhan 430079, China (e-mail: zhongyanfei@lmars.whu.edu.cn).

Color versions of one or more of the figures in this paper are available online at http://ieeexplore.ieee.org.

Digital Object Identifier 10.1109/TGRS.2013.2244095

The subpixel mapping technique introduced by Atkinson [6] can obtain the subpixel location of each class in a pixel by dividing a pixel into subpixels. These subpixels are assigned to different classes by subpixel mapping, with the constraint that the total number of subpixels of a given class is directly proportional to the percentage cover of that class for the original larger pixel [6]. By the subpixel mapping technique, a classification map with a finer resolution can be obtained, based on the fraction of the soft classification or spectral unmixing.

Before the concept of subpixel mapping was introduced by Atkinson, some other methods [7] had already been proposed to produce a fine map from a coarse map. After that, many methods were proposed based on spatial dependence [6], as proposed by Atkinson in 1997, which refers to the tendency for spatially proximate observations of a given property to be more alike than more distant observations. Atkinson considered that there are two basic types of algorithms for subpixels mapping [8]. The items in one type are the regression-type algorithms, such as the geostatistical methods [9]–[11], extensions of the linear mixture model [12] and the feed-forward back-propagation artificial neural network [13]–[15]. The items in the other type are based on spatial optimization, such as the pixel-swapping algorithm [16]–[18], Hopfield neural network [19]–[21], genetic algorithms [22] and differential evolution [23]. Furthermore, the spatial AC [24], Markov random fields [25]–[27] and a borderline segmentation technology [28] have also been proposed to tackle the subpixel mapping problem.

For the mixed pixel problem, Fisher [29] suggested that it is actually composed of four types of pixels: discrete subpixel, boundary pixels, intergrade pixels and linear subpixels. However, many subpixel mapping approaches ignore the different inherent structures in mixed pixels and consider the mixed pixels as an identical type, for example, boundary-mixed pixels or linear subpixels. The boundary-mixed pixels are the most common type in remotely sensed images. Furthermore, the linear subpixel phenomenon is also very important for remote-sensing image interpretation [29]. For example, it is important for land-cover classes with linear subpixel features, such as roads and rivers. Most methods can perform well for boundary-mixed pixels. For linear subpixels, an improved pixel-swapping algorithm, namely, linearized PSA, has been proposed to map rural linear land-cover features [17]. However, the type of mixed pixel cannot be determined automatically, and boundary-mixed pixels and linear subpixels may exist for the same class, so this method is limited to land-cover classes that contain only the linear subpixel type.

At present, most algorithms assume that only one type of mixed pixel, either boundary-mixed pixel or linear subpixel, exists for a particular land-cover class, which is not realistic. The critical problem is determining the different types of mixed pixels adaptively and implementing the corresponding approaches for the different types of mixed pixels.

To solve the problem mentioned above, an adaptive subpixel mapping algorithm based on a multiagent system (MAS) for remote-sensing imagery (MASSM) is proposed. In the proposed algorithm, two types of mixed pixels (boundary pixels and linear subpixels) are synchronously considered by utilizing the abilities of self-adaption and global optimization of the MAS. The MAS is a community of individual agents cooperating to achieve a prescribed system goal, with the advantage of distributed and concurrent problem solving [30], [31]. Due to the excellent performance in parallel processing and global optimization, MASs have been widely used in a variety of fields, such as image segmentation [32], [33], air traffic control [34], [35], electronic commerce [36], [37] and policy modeling [38].

Although MASs have been widely used, there are still few reports about their application in subpixel mapping due to the complexity of remote-sensing imagery. To utilize the advantages of distribution and global optimization for an MAS in subpixel mapping, different agents should be designed to detect features in mixed pixels and implement the corresponding subpixel mapping processing. To detect the two types of mixed pixels (boundary pixels and linear subpixels), an adaptive feature detection agent is designed by calculating the maximum linearization index (MLI) for the mixed pixel. After the type of pixel (pure pixel, boundary-mixed pixel or linear subpixel) is determined, the corresponding subpixel mapping agent (pure subpixel mapping agent, boundary subpixel mapping agent or linear subpixel mapping agent) is created to implement operations, including diffusion and mapping. It should be noted that only mixed pixels need to be mapped. For a boundary-mixed pixel, a traditional AC is used to determine the labels of the subpixels. For a linear subpixel, however, as the width of the detected line is always larger than one pixel in traditional line detection methods, a linear subpixel feature cannot be reconstructed well with these methods. Therefore, a novel subpixel line mapping algorithm is proposed in the linear subpixel mapping agent to determine the subpixels, which make up the linear subpixel feature by extracting the center line in the fraction image. Finally, if conflicts arise between the different agents, such as the feature detection agent and the subpixel mapping agent, a decision agent is then used to determine the final distribution in the mixed pixel. With the global control of different agents, an optimal subpixel mapping result can be obtained. The experimental results with both artificial images and remote-sensing images indicate that the proposed algorithm outperforms the other two traditional algorithms in reconstructing the different structures in mixed pixels.

A short description of subpixel mapping and MASs is presented in Section II. Section III gives the details of adaptive subpixel mapping based on an MAS. Section IV analyzes the experimental results with three artificial images and two remotely sensed images. Finally, Section V concludes this paper.

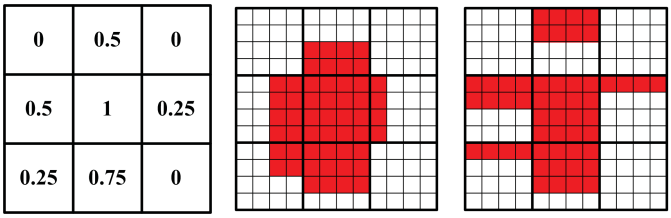

Fig. 1. Image of 3 × 3 coarse pixels and possible distributions (scale = 4, 2 classes). (a) Fraction image. (b) Optimal distribution. (c) Inferior distribution.

II. Background

A. subpixel Mapping

The key issue in subpixel mapping is how to determine an optimal subpixel distribution of each class in a pixel. Spatial dependence, as proposed by Atkinson in 1997, inspired from Tobler's first law [39], is the universal criterion, which refers to the tendency for spatially proximate observations of a given property to be more alike than more distant observations [6]. A coarser fraction image is obtained by a spectral unmixing technique, as the input image and each pixel is divided into × subpixels, where S represents the scale factor. The number of subpixels for each land-cover class is then determined by the abundances of the fraction image. Fig. 1 illustrates the principle of subpixel mapping and describes a simple example with two classes. In the fraction image, as shown in Fig. 1(a), assuming the scale fraction S is 4, a coarse pixel is divided into 16 (4 × 4) subpixels, and 0.5 in the fraction image means that 8 (16 × 0.5) subpixels belong to land-cover class 1. Fig. 1(b) and (c) describe two possible distributions of subpixels, and the former is superior to the latter, with higher spatial dependence.

Generally speaking, four kinds of features can be utilized in image processing: low-level visual features, local features, local-global features and biologically inspired features [40], [41]. However, these features are always based on the assumption that all pixels in the image are pure pixels, which is unreasonable in remotely sensed images. Fisher [29] suggested that there are four types of mixed pixels in remotely sensed images (see Fig. 2), as follows [42].

1) Small subpixel objects: the size of the object is smaller than the size of the pixel.
2) Boundary pixels: the sizes of two or more land-cover classes on the ground may be larger than the sizes of the pixel, but parts of their boundaries lie in a single pixel.
3) Intergrade pixels: a pixel allocates a space for a transition from a cluster of one class to a cluster of another class.
4) Linear subpixels: the length of a land-cover class may be longer than a pixel but its width is thinner, and the land-cover class runs through a pixel. Many subpixel mapping methods have been proposed to tackle the different types of mixed pixels: subpixel objects [43],

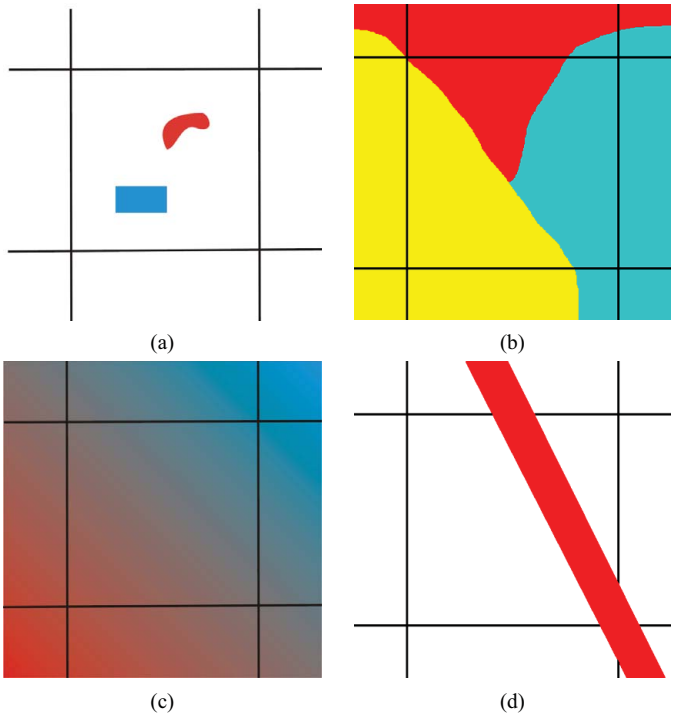

Fig. 2. Four causes of mixed pixels. (a) Small subpixel objects (a house or tree). (b) Boundaries between two or more mapping units (field-woodland boundary). (c) Intergrade between central concepts of mappable phenomena (ecotone). (d) Linear subpixel objects (a road or river) [28].

[44], boundary pixels [16], [24], [28], intergrade pixels and linear subpixels [17], [18].

Many of the subpixel mapping methods are based on the spatial dependence assumption, as proposed by Atkinson [6]. Given this assumption, only the boundary-mixed pixel and linear subpixel types satisfy this assumption. When it comes to the subpixel objects and intergrade pixels, it is hard to determine the distribution without auxiliary information [42].

Many methods have been proposed to solve the problem of subpixel mapping in a boundary-mixed pixel or linear subpixel; however, they assume that all mixed pixels belong to the same class, which is obviously unrealistic. For example, if the width of a road is greater than one pixel, the type of mixed pixel may be a boundary-mixed pixel, otherwise the type is a linear subpixel. To map the two kinds of mixed pixels simultaneously, an adaptive method is necessary that can detect the different types of mixed pixels automatically and conduct the corresponding subpixel mapping method.

B. Multiagent Systems

Multiagent systems are systems composed of multiple interacting computing elements known as agents [45]. An agent is an encapsulated computer system that is situated in some environment, either geometrical or numerical, and is capable of flexible, autonomous action in that environment, in order to meet its design objectives [46]. It has characteristics such as autonomy, social ability, reactivity and proactivity [47]. Agents have been widely applied in computer vision and image processing, for applications such as image segmentation [31], [48] and feature extraction [49].

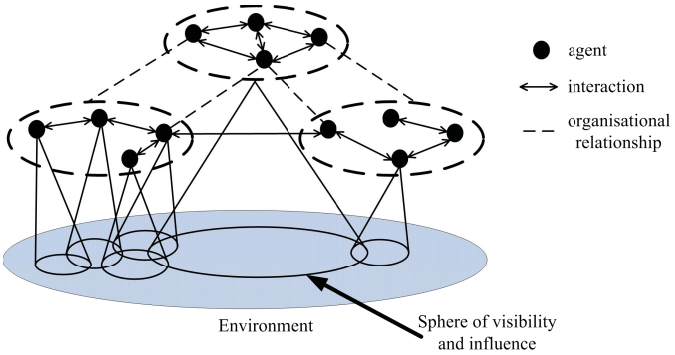

Fig. 3. Typical structure of a multiagent system.

Agents locally interact with their environments in the course of problem solving. Responding to different local constraints received from their task environments, agents can select and exhibit different behavioral patterns. The behavioral patterns of agents may be predefined and activated by certain conditions from the agent environment [31]. Fig. 3 illustrates the typical structure of an MAS [50]. The system contains a number of agents that interact with one another through communication. Every agent has control over parts of the environment, but the problem solving relies on the coordination and interaction of different agents. In an MAS, an agent is influenced by the environment and other agents. It has to coordinate with the others to meet their objectives. However, sometimes the objective of an agent may be different from the others' and conflict may occur in the pursuit of its own goal. In such cases, a consultation mechanism is necessary for conciliating the contradiction, in order to achieve the purpose.

With the ability of self-adaptation, an MAS can deal with the different structures in mixed pixels. Our proposed method based on an MAS is motivated by the intention of identifying different structures in mixed pixels with corresponding algorithms. The intention is not to simply apply every algorithm on each pixel, but to select an appropriate algorithm, varying automatically with the detected features and environment. In addition, agents may conflict with others, and it is important to coordinate agents with different objectives to obtain the optimal global solution.

III. Adaptive Subpixel Mapping Based on a Multiagent System

With the advantages of distribution and global optimization, this paper proposes an adaptive subpixel mapping algorithm based on an MASSM to conduct subpixel mapping.

To apply an MAS to subpixel mapping, MASSM is designed to consist of three layers, as follows. In the first layer, feature detection agents (FDAs) are used to detect the different structures in mixed pixels, including boundary-mixed pixels and linear subpixels. The middle layer consists of subpixel mapping agents (SMAs) that reconstruct features with different subpixel mapping algorithms based on FDAs. The highest level consists of decision agents (DAs) that coordinate the contradictions between FDAs and SMAs.

In MASSM, the set of agents A, $A = \{A^F, A^M, A^D\}$, consists of all the agents, where A^F represents the FDAs, A^M

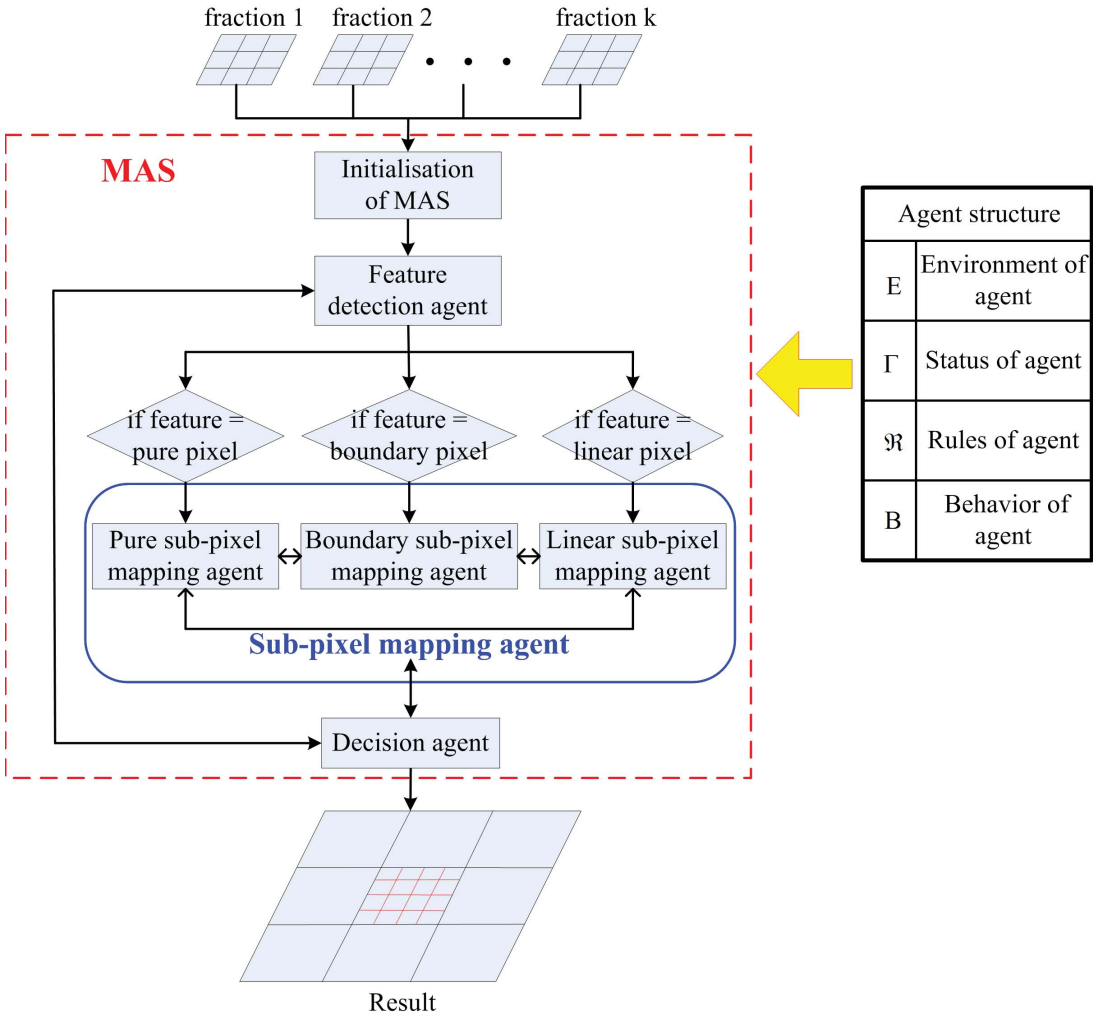

Fig. 4. Framework of the proposed method.

is the SMAs, and A^D is the DA. To describe the set of agents A with these different kinds of agents, $A = \{A^F, A^M, A^D\}$, a universal structure of the agent set is defined. Taking A^F as an example, the structure can be represented by $< \mathrm{E}^F, \Gamma^F, \Re^F, B^F >$:

1) E^F is the environment information of agent A^F;
2) Γ^F is the status of current agent A^F;
3) $\Re^F$ is the rule library of A^F;
4) B^F is the set of possible behavioral patterns ofA^F.

Furthermore, A^{F^+} is the offspring agent of A^F, and A^{F^-} is the parent agent.

In the subpixel mapping problem, the fraction image can be represented as $E = \{P_{i,j} | i \in [0, m-1]; j \in [0, n-1]\}$, in which $P_{i,j} = \{P_{i,j}(c) | c \in [1, C]\}$ is the pixel with label (i, j), $P_{i,j}(c)$ is the fraction value of pixel $P_{i,j}$ for class c, (m, n) is the height and width of the fraction image, and C is the band number. The steps of the proposed approach can be summarized as follows.

Generally speaking, there are two ways of initialization for the FDAs. One way is to spread the agents equally on the image, and the other is to spread them randomly. In this paper, we have adopted the former strategy. The other strategy will be experimented on in the parameter analysis section to test the impact of initialization on the accuracy of the proposed method. Every agent A^F communicates with the environment E^F, and different types of mixed pixels can be detected by E^F and the rule library $\Re^F$. In this paper, only the boundary-mixed pixels and linear subpixels are considered, which means that a mixed pixel without a linear subpixel feature will be labeled as a boundary-mixed pixel. This task can be simplified by detecting if there is a linear subpixel feature in the mixed pixel.

For different types of mixed pixels, specific SMAs will be created respectively. As only two types of mixed pixels are taken into consideration, SMAs may contain three different types of agents: 1) pure subpixel mapping agent; 2) boundary subpixel mapping agent; and 3) linear subpixel mapping agent.

As the sphere of influence for different agents may overlap with each other, a decision agent is necessary for conciliating the contradictions of FDAs and SMAs.

The general flow is as shown in Fig. 4. In this paper, the impact of parameter N, the number of original FDAs in the

fraction image, and the life threshold T of the SMAs are also taken into account.

The process of MASSM is as follows.

A. Feature Detection Agent

To reconstruct the different features in a mixed pixel, the type of mixed pixel should be first determined. In this step, a feature detection agent is utilized to detect the type of subpixel structure, where boundary pixels and linear subpixels are considered. As only the boundary-mixed pixel and linear subpixel are taken into consideration, the feature detection agent can be simplified as a linear subpixel feature detection agent.

Fig. 5 describes how to decide whether a linear subpixel feature exists in a mixed pixel. In this paper, D is the side length of the square neighborhood, and is set as 5. Putting the grid into a uniform coordinate system and setting the origin at the upper left, then every pixel $P_{i',j'}$ will get a coordinate $(i'+0.5, j'+0.5)$. For example, the coordinate of pixel $P_{0,0}$ at the upper left is represented as $(0.5, 0.5)$.

Assuming the agent A^F is located in the center pixel $P_{i,j}$, which has C classes, for every class c it may diffuse to neighboring pixels that have the same class c. The environment $E^F = \Omega^F \cup \{\varepsilon^F\}$ indicates the neighboring pixel Ω^F of the current agent A^F, and the pixel ε^F the agent occupies is defined as

$$\begin{aligned} E^F &= \left\{ P_{i',j'} \,\middle|\, |i'-i| \le \frac{D}{2} \wedge |j'-j| \le \frac{D}{2} \right\} \\ \Omega^F &= \left\{ P_{i',j'} \,|(i' \ne i \vee j' \ne j) \right. \\ &\qquad \left. \wedge \left(|i'-i| \le \frac{D}{2} \wedge |j'-i| \le \frac{D}{2} \right) \right\} \\ \varepsilon^F &= P_{i,j}. \end{aligned} \tag{1}$$

The status $\Gamma^F = \{\mathrm{CR}^F, \mathrm{PL}^F, \mathrm{flag}^F\}$ indicates the control area CR^F of pixel $P_{i,j}$ and the pixel set PL^F of agent A^F and its offspring agents, as illustrated in Fig. 5, which are labeled with yellow, and the flag^F shows the type of $P_{i,j}$. If $P_{i,j}$ is a mixed pixel, $\mathrm{flag}^F = 1$, otherwise $\mathrm{flag}^F = 0$. The $\wedge$ symbol means the "AND" operator, and the $\vee$ symbol represents the "OR" operator.

To determine if there is a linear subpixel feature, every possible line across the center pixel should be verified. The decision procedure involves three steps.

First, find all possible lines. Any line in the picture can be represented by pixels it passes through, and the task is to find all the pixel sets. Lines between L_a and L_c occupy the same pixels as L_c and, therefore, lines between L_c and L_d can delegate all possible lines. Then, the following formula can be used to represent all the lines as L_λ

$$L_\lambda : x = y \times \tan\beta_\lambda + C, \quad \beta_\lambda = \theta + \lambda\tau. \tag{2}$$

In (2), β_λ is the angle between the current possible line L_λ and L_b. $\beta_\lambda \in \{\beta \,|-\theta \le \beta \le \theta\}$ and $\theta = \arctan(D)$.

Second, the line L_λ rotates from L_c to L_d with a fixed angle τ, and the corresponding pixel set PL_λ^F, which represents the line L_λ, can be determined by examining if line L_λ interacts with the control area CA^F of pixels in E^F as (3). As illustrated in Fig. 5, the line L_e can be represented with pixels, which are labeled with yellow

$$\begin{aligned} \mathrm{CA}^F &= \left\{ \mathrm{AR}_{i',j'} \middle| (i' \to (i'+1)) \right. \\ &\qquad \left. \wedge (j' \to (j'+1)),\ (i', j') \in E^F \right\} \\ \mathrm{PL}_\lambda^F &= \{ P_{i',j'} \,|\mathrm{AR}_{i',j'} \wedge L_\lambda \ne \emptyset \}. \end{aligned} \tag{3}$$

The CA^F is the control area of pixel $P_{i,j}$, and it is the set of all $\mathrm{AR}_{i',j'}$. In the coordinate system, every pixel is represented with a grid square, which is represented as $\mathrm{AR}_{i',j'}$ for pixel $P_{i',j'}$. The region of the grid square for pixel $P_{i',j'}$ is $(i' \to (i'+1)) \wedge (j' \to (j'+1))$.

The behavioral pattern $B^F = \{B_P^F, B_B^F, B_L^F\}$ shows three behaviors decided by $\Re^F$. B_P^F, B_B^F, and B_L^F are the behaviors to create a pure SMA A_P^M, boundary SMA A_B^M or linear SMA A_L^M, in pixel $P_{i,j}$, respectively.

Finally, the defined rule library and the behavioral pattern can be used to determine if there is a linear subpixel feature. The rule library $\Re^F$ and the behavioral pattern B^F can be described as

$$\Re^F : B^F \to \begin{cases} B_P^F & \mathrm{flag}^F = 0 \\ B_L^F & \mathrm{flag}^F = 1 \ \&MLI \ge \rho \ \&G_{\lambda'}(c') \ge D \\ B_B^F & \text{else.} \end{cases} \tag{4}$$

In (4), MLI is the maximum linearization index, which is calculated by (5) and (6), and ρ is the threshold to determine if there is a linear subpixel feature. In this paper, ρ was set to the experiential value of 0.5. $G_{\lambda'}(c') \ge D$ is used to make sure that only lines that go through the center pixel are thought to be linear subpixel features, to avoid excess determination

$$\mathrm{MLI} = \psi_{\lambda'}(c'), \quad \exists\, \lambda', c' : \psi_{\lambda'}(c') = \max\{\psi_\lambda(c), c \in [1, C]\} \tag{5}$$

where $\psi_\lambda(c)$ means the possibility of a line existing for class c

$$\begin{aligned} \psi_\lambda(c) &= \frac{G_\lambda(c)}{H_\lambda(c)} \\ G_\lambda(c) &= \sum_{P_{i',j'} \in PL_\lambda^F} g_{i',j'} \\ g_{i',j'} &= \begin{cases} 1, & P_{i',j'}(c) > 0 \\ 0, & \text{else} \end{cases}, \quad P_{i',j'} \in PL_\lambda^F \\ H_\lambda(c) &= \sum_{P_{i',j'} \in E^F} h_{i',j'} \\ h_{i',j'} &= \begin{cases} 1, & P_{i',j'}(c) > 0 \\ 0, & else \end{cases}, P_{i',j'} \in E^F \end{aligned} \tag{6}$$

where E^F is the environment information of agent A^F, as defined in (1); PL_λ^F is the pixel set, which represents the line L_λ, which can be determined by (3); $G_\lambda(c)$ is the number of pixels in PL_λ^F for class c whose fraction values are greater than zero; and $H_\lambda(c)$ is the number of pixels in E^F for class c whose fraction values are greater than zero.

Although the linear subpixel feature detection algorithm can determine whether there is a linear subpixel feature, it cannot ensure what the exact angle is, due to lots of lines occupying

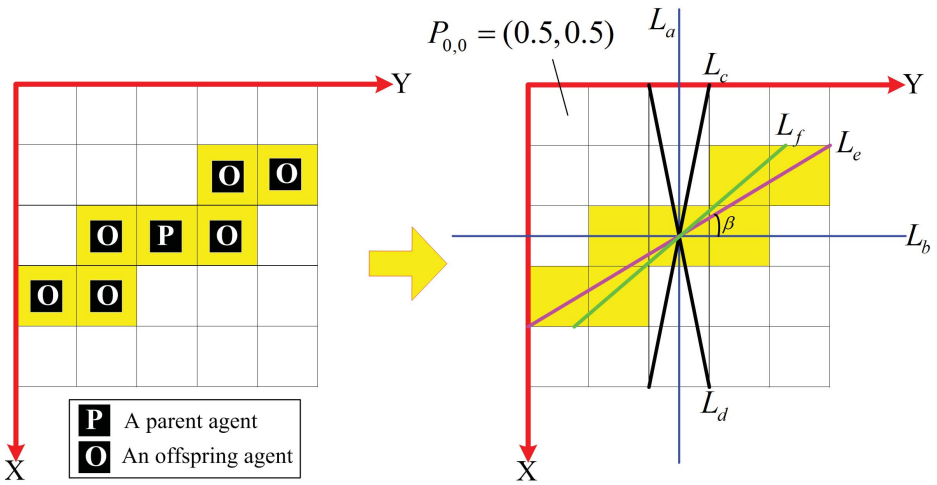

$$\theta = \arctan(D),\ D \text{ is the side length of the square neighborhood}$$

$$-\theta \le \beta \le \theta,\ \beta \text{ is the angle between } L_e \text{ and } L_b$$

$$L_a : Y = \frac{D}{2} \quad L_b : X = \frac{D}{2} \quad L_c : x = y * \tan(-\theta) + r_1$$

$$L_d : x = y * \tan\theta + r_2 \quad L_e : x = y * \tan\beta + r_3$$

Fig. 5. Illustration of a linear subpixel feature detection agent for class c.

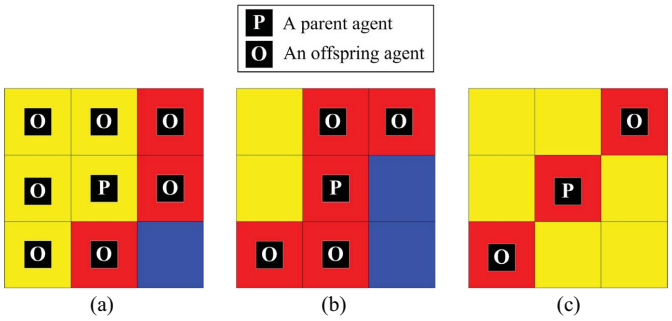

Fig. 6. Diffusion of different types of pixels. The yellow pixel is a pure pixel, which belongs to class c, the blue pixel is a pure pixel, which belongs to class w, and the red pixel is a mixed pixel that contains classes c and w. (a) Center agent in a pure pixel may diffuse to its neighboring pixels that contain the same class. (b) Center pixel is a boundary pixel, and the agent in it diffuses to the neighboring mixed pixels that have the same land-cover class as the center one. (c) Center pixel has a linear subpixel feature, and the agent in it will diffuse along the detected direction of the line.

the same pixel set. This is described in Fig. 5, where L_e and L_f occupy an identical pixel set. Therefore, a method to confirm the angle of line and diffuse the agent is essential. With regard to a mixed pixel that cannot be affirmed to be a linear subpixel feature component, it is considered to be a boundary-mixed pixel.

B. Mechanism of the subpixel Mapping Agent

Since the type of a mixed pixel has been determined by FDA, the corresponding subpixel mapping agent should be implemented for the different types of pixels. As mentioned before, a pixel may be a pure pixel, boundary pixel or linear subpixel. The subpixel mapping agent can be represented as $A^M = \{A_P^M, A_B^M, A_L^M\}$, where A_P^M is the pure subpixel mapping agent, A_B^M is the boundary subpixel mapping agent, and A_L^M is the linear subpixel mapping agent. For the agent A^M, which is found in a pixel $P_{i,j}$, the environment E^M can be described as

$$\begin{aligned} E^M &= \left\{P_{i',j'} \middle| |i'-i| \le 1 \wedge |j'-j| \le 1\right\} \\ \Omega^M &= \left\{P_{i',j'} \middle| (i' \ne i \vee j' \ne j) \right. \\ &\qquad \left. \wedge (|i'-i| \le 1 \wedge |j'-i| \le 1)\right\} \\ \varepsilon^M &= P_{i,j}. \end{aligned} \tag{7}$$

The status $\Gamma^M = \{\eta^M, \delta^M, f^M\}$ shows some attributes of agent A^M. The value of η^M indicates whether the current agent A^M is a parent agent or offspring agent. If A^M is a parent agent, $\eta^M = 1$, otherwise $\eta^M = 0$. The value of δ^M means the dominant class in the pixel, which should be assigned preferentially. f^M is the current life of A^M to control the diffusion.

1) Diffusion of Pure SMA: subpixel mapping is not required for a pure pixel; however, the diffusion of the agent in a pure pixel has an impact on the result of subpixel mapping for the neighboring mixed pixels.

For the agent A_P^M located in a pure pixel $P_{i,j}$, which belongs to class c, $\delta_P^M = c$. The behavioral pattern B_P^M indicates the diffusion of agent A_P^M. If the life $f_P^M < T$, the agent A_P^M may spread to its neighboring pixels, as Fig. 6 (a) depicts. The rule $\Re_P^M$ to determine the offspring agent set DF_P^M of agent A_P^M is described as

$$\Re_P^M : DF_P^M = \left\{ P_{i',j'} \middle| \begin{array}{l} (|i'-i| \le 1) \wedge (|j'-j| \le 1) \wedge \\ (P_{i',j'}(\delta_P^M) > 0) \wedge (P_{i',j'} \ne P_{i,j}) \end{array} \right\}. \tag{8}$$

It is obvious that the pure SMA may diffuse to mixed pixels, and it is assumed that a mixed pixel that contains an offspring pure SMA is a boundary-mixed pixel, and a boundary SMA will be created instead of the offspring pure SMA. Finally, every subpixel in center pixel $P_{i,j}$ will be assigned to class c.

2) Mapping With Boundary SMA: The boundary-mixed pixels consist of two types: one is determined by FDA and the other is the mixed pixel, which the offspring of pure SMA or boundary SMA locates in. For the boundary-mixed pixel $P_{i,j}$, which is determined by FDA, a boundary SMA A_B^M is created. In the status Γ^M, $\eta_B^M = 1$ and $\delta_B^M = k$ ($P_{i,j}(k) = \max\{P_{i,j}(c), c \in [1, C]\}$). For the latter type of boundary-mixed pixel, $\eta_B^M = 0$ and $\delta_B^M = \delta^{M^-}$, where δ^{M^-} belongs to the parent agent of A_B^M. The behavioral pattern $B_B^M = \{B_{BD}^M, B_{BM}^M\}$ shows two behaviors decided by $\Re_B^M = \{\Re_{BD}^M, \Re_{BM}^M\}$. B_{BD}^M is the behavior of diffusion of agent A_B^M, and B_{BM}^M is the implementation of subpixel mapping for pixel $P_{i,j}$. Under the rule library $\Re_{BD}^M$, agent A_B^M may diffuse to the neighboring mixed pixels, as Fig. 6(b) described by (9). The life of the offspring agent may be $f_B^M + 1$

$$\Re_{BD}^M : DF_B^M = \left\{ P_{i',j'} \left| \begin{array}{l} (|i'-i| \le 1) \wedge (|j'-j| \le 1) \wedge \\ (0 < P_{i',j'}(\delta_B^M) < 1) \wedge (P_{i',j'} \ne P_{i,j}) \end{array} \right. \right\}. \tag{9}$$

After that, the rule $\Re_{BM}^M$ to implement subpixel mapping employs the attraction model as (10). It estimates the class of subpixels according to the class proportion of its neighboring pixels by calculating the attraction values of the different classes

$$\Re_{BM}^M : p_{a,b}(c) = \text{Avg} \left\{ \frac{P_{i',j'}(c)}{d(p_{a,b}, P_{i',j'})} \left| \begin{array}{l} (|i'-i| \le 1) \\ \wedge (|j'-j| \le 1) \\ \wedge (P_{i',j'} \ne P_{i,j}) \end{array} \right. \right\} \tag{10}$$

$$d\left(p_{a,b}, P_{i',j'}\right) = \sqrt{\left[a + 0.5 - S\left(i' + 0.5\right)\right]^2 + \left[b + 0.5 - S\left(j' + 0.5\right)\right]^2}. \tag{11}$$

1) $p_{a,b}(c)$ is the attraction value for subpixel $p_{a,b}$ and class c;
2) $P_{i',j'}(c)$ is the fraction value for pixel $P_{i',j'}$ and class c;
3) $d(p_{a,b}, P_{i',j'})$ is the distance for subpixel $p_{a,b}$ and pixel $P_{i',j'}$.

It is illustrated in Fig. 7 and defined as (11), in which coordinates of the subpixel and pixel should be integrated into the same coordinate system. In addition to the Euclidean space, some other metric learning algorithms [51], [52] can be utilized in the design of the subpixel mapping agent.

The attraction value of every subpixel for the predominant class can be calculated by (10), and subpixels assigned to that class can be determined by constraint of the abundance, and the attraction values. The rest of the classes are equal to each other, and every class will get a subpixel by turn, with the limitations of abundance of the remaining classes, and attraction values of the unlabeled subpixels for the other classes.

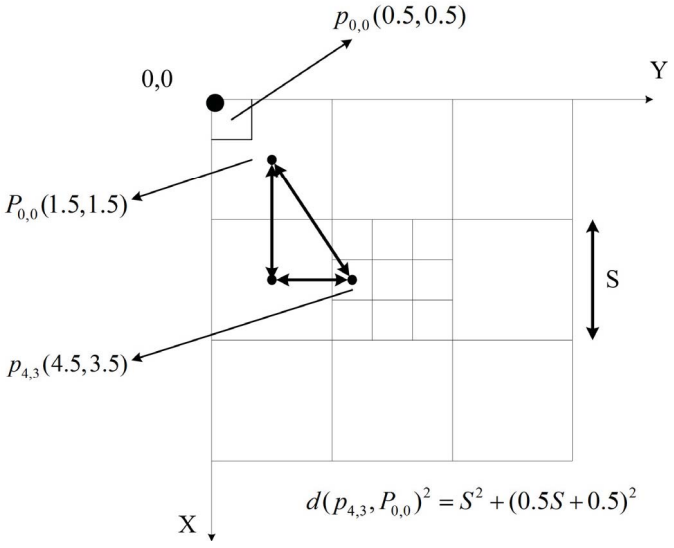

Fig. 7. Illustration of the labeling of pixels and subpixels, the coordinate system, and the distance calculation between pixels and subpixels.

3) Mapping With Linear SMA: After a linear subpixel feature is detected by FDA in a mixed pixel $P_{i,j}$ for class c, the linear SMA A_L^M is created. No matter whether it is a parent agent or offspring agent, the same diffusion mechanism will be selected.

The behavioral pattern $B_L^M = \{B_{LD}^M, B_{LM}^M\}$ shows two behaviors, decided by $\Re_L^M = \{\Re_{LD}^M, \Re_{LF}^M, \Re_{LM}^M\}$. B_{LD}^M is the behavior of diffusion of agent A_L^M, and B_{LM}^M is the implementation of subpixel mapping.

To implement the subpixel mapping, a center line should be determined first, as Fig. 8 illustrates. Fig. 8(a) shows the fraction values of pixels of $P_{i,j}$ and its neighboring pixels for class c. First, a binary operation should be implemented to obtain a binary image by comparing with the threshold of abundance, which is set as zero. Then, a line-fitting algorithm is applied to the binary image to extract a center line. Finally, pixels in E_L^M, except the two endpoints, should be mapped by the distance of the subpixel to the center line.

To fit a line, a least-squares-based line-fitting method is employed. Put the 3×3 grid into a coordinate system and set the origin point at the top left. Then, every pixel $P_{i',j'}$ of set E_L^M and subpixel $p_{a,b}$ in $P_{i',j'}$ will get a uniform coordinate, as depicted in Fig. 8 by (12)

$$\begin{aligned} P_{i',j'} &= (X_{i'}, Y_{j'}) = (S \times (i' + 0.5), S \times (j' + 0.5)) \\ p_{a,b} &= (x_a, y_b) = (a + i' \times S + 0.5, b + j' \times S + 0.5). \end{aligned} \tag{12}$$

In Fig. 8, the resize factor S is 4 and, therefore, the coordinate of the top left subpixel is $p_{0,0} = (0.5, 0.5)$, while that of the top left pixel is $P_{0,0} = (2, 2)$. In the procedure of line fitting, only coordinates of pixels are used. As Fig. 8 declares, a linear subpixel feature has been detected by the previous FDA, and pixels that contain the class c form the linear subpixel feature. The rule to implement the subpixel mapping line can be represented as

$$\text{Line-fitting rule } \Re_{LF}^M : \begin{cases} l_{xy} = 0, & y = Ax + B \\ l_{xy} \ne 0, & x = z. \end{cases} \tag{13}$$

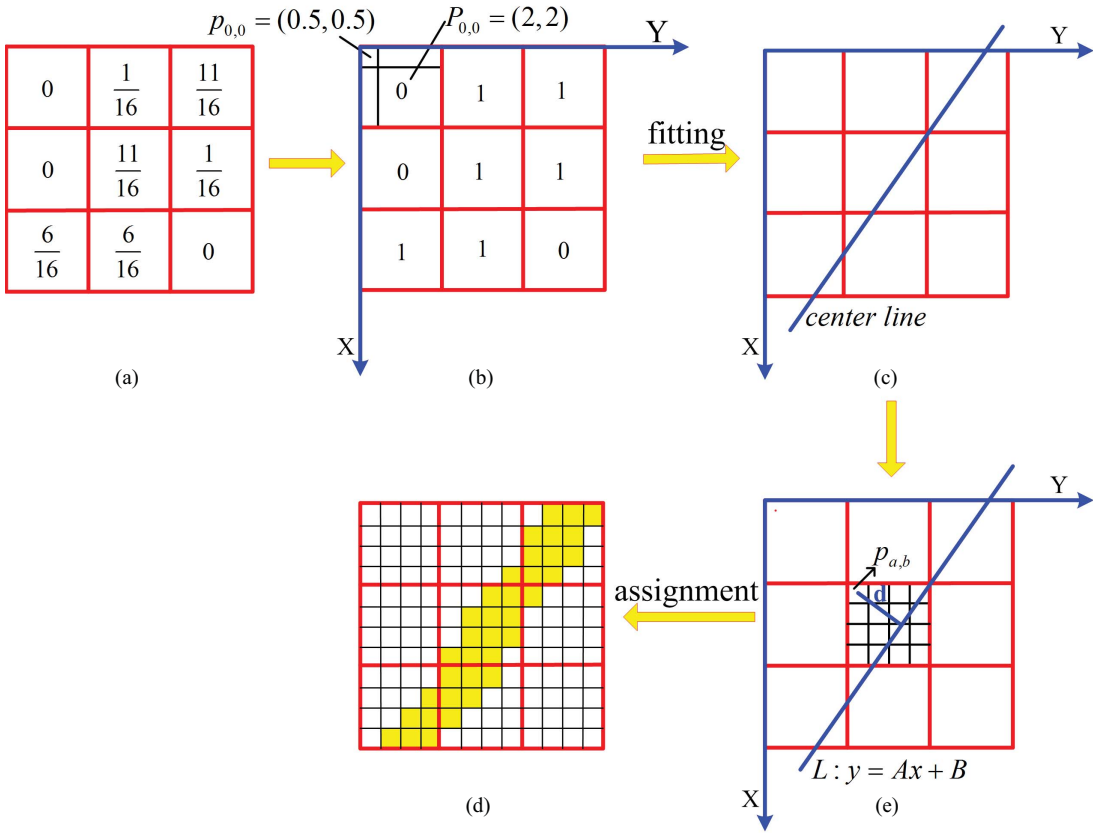

Fig. 8. Linear subpixel mapping agent used to reconstruct a linear subpixel feature. (a) Fraction image of class c. (b) Diffusion of linear SMA. (c) Fitting a center line with the position of the SMAs. (d) Calculation of the distance from the subpixel to the center line. (e) Linear feature-mapping result.

Assuming that there are ω pixels in set E_L^M, then the center line can be determined by

$$\begin{aligned} &\bar{X} = \sum X_{i'} \Big/ \omega; \quad \bar{Y} = \sum Y_{j'} \Big/ \omega \\ &l_{xx} = \sum (X_{i'} - \bar{X})^2 \Big/ \omega; \quad l_{yy} = \sum (Y_{j'} - \bar{Y})^2 \Big/ \omega \\ &l_{xy} = \sum (X_{i'} - \bar{X})(Y_{i'} - \bar{Y}) \Big/ \omega \\ &\begin{cases} A = \left[l_{yy} - l_{xx} + \sqrt{(l_{yy} - l_{xx})^2 + 4l_{xy}^2} \right] \Big/ 2l_{xy} \\ B = \bar{Y} - A\bar{X} \\ z = \bar{X}. \end{cases} \end{aligned} \tag{14}$$

Then, the offspring agent set DF_L^M of agent A_L^M, which the center agent A_L^M may diffuse to, should be determined with rule $\Re_{LD}^M$. The rule to determine DF_L^M is as follows. Let $L_{i',j'}$ be the line connecting the neighboring pixel $P_{i',j'}$ and center pixel $P_{i,j}$. As the position of the line has been figured out, the angle $\alpha_{i',j'}$ between L and $L_{i',j'}$ can be calculated. The two pixels with the smallest two angles will be selected as the endpoints of the line, and the center agent will diffuse to them, as illustrated in Fig. 9

$$\Re_{LD}^M : DF_L^M = \left\{ P_{i'',j''}, P_{i''',j'''} \middle| \begin{matrix} \alpha_{i'',j''} \le \alpha_{i''',j'''} \le \alpha_{i',j'} \\ P_{i'',j''} \in E_L^M, P_{i''',j'''} \in E_L^M \end{matrix} \right\}. \tag{15}$$

After the direction of diffusion has been determined, the distribution of classes in the pixels, except the two endpoints, should be determined. The rule for mapping the center pixel and neighboring pixels is to calculate the distance of subpixel $p_{a,b}$ in pixel $P_{i',j'}$ and line L by (16), in which $L : y = Ax + B$. Fig. 8(d) illustrates the distance of the subpixel to the center line. subpixels in pixel $P_{i',j'}$ will be sorted by the distances, and subpixels that are near to the line will be labeled as the target class, with the constraint of abundance. For the rest of the subpixels of pixel $P_{i',j'}$, the attraction values of the subpixels and neighboring pixels will determine the attribution of every other subpixel, as in the way of subpixel mapping of the boundary feature

$$\text{Class determination rule } \Re_{LM}^M : d_{a,b} = \frac{|A * X_a + B - Y_b|}{\sqrt{A^2 + B^2}}. \tag{16}$$

C. Decision Agent

Because of the existence of different types of mixed pixels, an agent with a single function cannot obtain the best result. Therefore, the MAS is employed to solve the problem. However, agents in the MAS cannot always keep up and sometimes may conflict with others, as they have their own particular aims, besides the common objective. In order to maximize the individual target, an agent may hinder the process of other agents. Therefore, a consultation mechanism is essential to resolve the conflict so that the common goal of the MAS can be fulfilled. During the diffusion of a SMA, it may run up

TABLE I
RULE $\Re^D$ AND THE BEHAVIORAL PATTERN B^D OF AGENT $A_D^{M'}$

$A^{M'}$ \ pf	Pure Pixel	Boundary Pixel	Linear Pixel
Pure SMA	$A_P^{M'} \Rightarrow A_P^{M'}$	$A_P^{M'}$ die	$A_P^{M'}$ die
Boundary SMA	$A_B^{M'}$ die	$A_B^{M'}$ die	$A_B^{M'} \Rightarrow$ $A^F \Rightarrow \begin{cases} A_B^{M'} \\ A_L^M \end{cases}$
Linear SMA	$A_L^{M'}$ die	$A_L^{M'} \Rightarrow$ $A^F \Rightarrow \begin{cases} A_B^M \\ A_L^{M'} \end{cases}$	$A_L^{M'}$ die

against some pixels that have been handled by other SMAs. For these controversial areas, a decision agent A^D is used to determine the optimal result.

In this paper, the environment E^D of agent A^D in pixel $P_{i,j}$ can be defined as $E^D = P_{i,j}$, and the status $\Gamma^D = \{A^{M'}, pf\}$, in which $A^{M'}$ is the current subpixel mapping agent, which diffuses to pixel $P_{i,j}$, and pf is the type of pixel $P_{i,j}$, which was determined previously. $A^{M'}$ can be pure SMA, boundary SMA or linear SMA. pf can be pure pixel, boundary-mixed pixel or linear subpixel. Table I shows the rule $\Re^D$ and behavioral pattern $B^D$to implement agent A^D with different combinations of $A^{M'}$ and pf.

Most contradictions happen between linear SMAs and boundary SMAs. If two SMAs conflict with each other and one of them is a linear SMA, the linear subpixel feature detection agent will be utilized by the decision agent to determine what exactly the type of mixed pixel is. Then, similar steps will be taken as previous. However, if the two conflicted SMAs are both boundary SMAs or linear SMAs, then the rule of "first come, first served" is used.

Generally speaking, a linear subpixel is given priority over other types of pixels. In this way, potential linear subpixel features can be preserved and reconstructed as soon as possible.

D. Stopping Condition

Parameters such as the number N of original FDA in the fraction image and the life threshold T of SMA control the implementation of MAS in the subpixel mapping, lower values of which may result in a portion of the pixels being ignored. To avoid this, a compromised way is to apply an AC on unsettled pixels after all the agents in the image have died out.

IV. EXPERIMENTS AND ANALYSIS

The subpixel mapping algorithm should ideally be applied on a fraction image generated by the spectral unmixing of a remotely sensed image. However, in this way, errors due to soft classification and some other processes are introduced in the assessment of the subpixel mapping method. To evaluate subpixel mapping algorithms solely, synthetic images are created by degrading a classification map to a simulated fraction image, by the use of a resize factor. In this way, the original classification map can be used as a reference image to evaluate the different subpixel mapping methods. However, to confirm

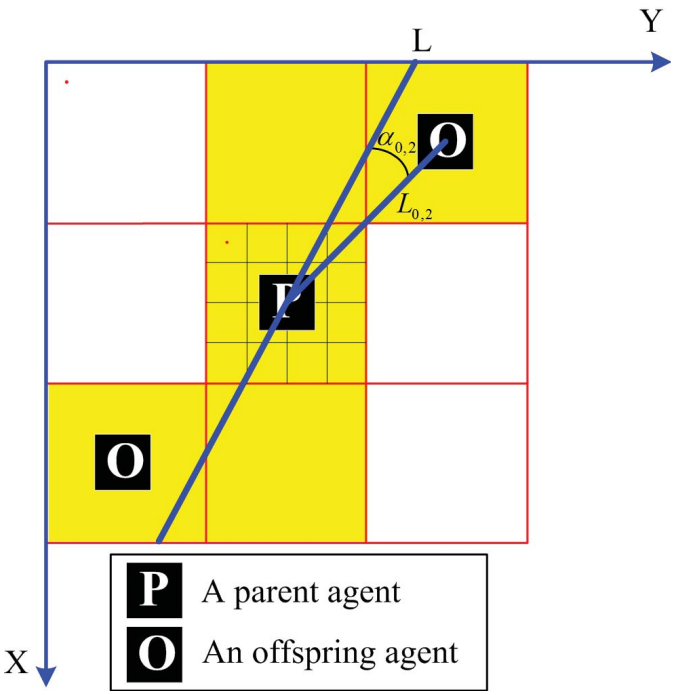

Fig. 9. Diffusion of the linear SMA. L is the line fitted by yellow pixels, and $\alpha_{0,2}$ is the angle between L and $L_{0,2}$.

the reliability of the proposed method, another procedure to implement the subpixel mapping is applied to the remotely sensed images to further test the effectiveness of our proposed method.

To verify the performance of the proposed algorithm, three artificial images and two remotely sensed images are employed. Artificial images, including an image containing only boundary features, an image containing only linear subpixel features, and an image containing both features, are used to facilitate the design and development of the algorithm. Another two remotely sensed images are employed to test the validation of the algorithm on more complex imagery. Hard classification (HC), a BP neural network (BP) and an AC (AM) are used to compare the results with the proposed algorithm, and the accuracy of the different methods is provided.

In this paper, two novel recently proposed indices, quantity disagreement (QD) and allocation disagreement (AD) [53], are utilized to evaluate the subpixel mapping results of the different subpixel mapping methods. The QD is the amount of difference between the reference map and a comparison map that is due to the less than perfect match in the proportions of the categories. The AD is the amount of difference between the reference map and a comparison map that is due to the less than optimal match in the spatial allocation of the categories, given the proportions of the categories in the reference and comparison maps. The calculation of the two components is described in [53]. Moreover, the overall accuracy (OA) is also utilized. In addition, as the subpixel mapping methods focus on the mixed pixel problem, other kind of indices, adjusted OA [23], adjusted QD and adjusted AD, are also utilized. These indices are calculated only for mixed pixels, and they

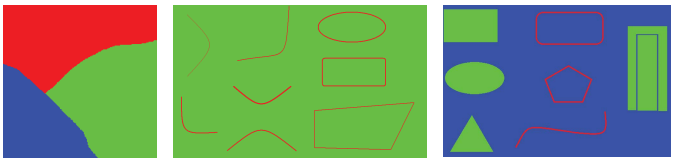

(a) (b) (c)

Fig. 10. Three artificial classification images for testing. (a) 200 × 200 image with only boundary features, and $S = 10$. (b) 900 × 540 image with only linear subpixel features, and $S = 4$. (c) 540 × 360 image with both boundary features and linear subpixel features, and $S = 6$.

ignore the subpixels that have a pure pixel as parent in the fine-resolution image.

In addition, to test the statistical significance of the differences in accuracy for two classification results, the McNemar's test [54] is used to compare the misclassification rates with the different methods. For the two classification maps C_1 and C_2, the McNemar's test compares the number of pixels misclassified inC_1, but not in $C_2(M_{12})$, with the number of pixels misclassified in C_2 while not in $C_1(M_{21})$. If $M_{12}+M_{21} \geq 20$, the X^2 can be considered as a chi-squared distribution (with one degree of freedom) [55], [56] as (17)

$$X^2 = \frac{(|M_{12} - M_{21}| - 1)^2}{M_{12} + M_{21}} \approx \chi_1^2. \tag{17}$$

The McNemar's test accepts the hypothesis that the two classification methods have the same error rate at significance level α if the value is less than or equal to $\chi^2_{\alpha,1}$ [57]. In other words, if the McNemar's value is greater than $\chi^2_{\alpha,1}$, the two classification algorithms are significantly different. In this paper, the significance level α is set as 0.05, which means $\chi^2_{\alpha,1} = 3.841459$.

A. Experiment 1—Artificial Images

The artificial images are illustrated in Fig. 10. To assess the performance of the proposed method in reconstructing different features in mixed pixels, three artificial images with different structures are tested. Fig. 10(a) contains three land-cover classes labeled with different colors, and only the boundary feature is considered. Given the size of the image, the resize factor can be set to 2, 4, 5, 8, 10, etc. In this experiment, it is set to 10. Fig. 10(b) contains only linear subpixel features whose widths vary from one to three pixels to form linear subpixels, given the resize factor of 4. Fig. 10(c) contains three land-cover classes, and both a boundary feature and linear subpixel feature are included. To construct the linear subpixel features, the widths of lines are set to two to three pixels, given the resize factor of 6.

The three images are tested by HC, the BP neural network, the AC and the proposed method, separately, and the results are illustrated in Fig. 11. As the size of the images is too large to interpret accurately, a partial enlarged view is provided for each method. For data 1, the result of MASSM is similar to that of AM, and HC has the worst performance. However, MASSM does well in some details, as seen in Fig. 11(j1). Compared with the reference classification map, the detailed maps of the different methods show that MASSM has a better effect than the other two methods in reconstructing boundary pixels. For data 2, the detailed map is cut from the polygon in the lower right corner. The lines of the detailed maps for MASSM are continuous, while for the other three methods, however, they are fractured. It is obvious that MASSM outperforms the other three methods, and the linear subpixel features can be reconstructed effectively. When it comes to data 3, the same conclusion can be made. Although the result of MASSM for data 3 is not as good as data 2, because of the complexity, it is still better than the others. The results of the BP and AM methods cannot extract a complete line; however, MASSM can achieve this.

The quantitative indices lead to the same conclusion as the visual assessment. Table II shows the accuracy of the different methods for the artificial images. For the linear subpixel features in data 2, the MASSM method has the best performance, and it decreases the adjusted AD from 0.173 and 0.132 to 0.108, when compared with BP and AM, respectively. Complete linear subpixels are not easily mapped with BP and AM, while MASSM is more suitable because of the adaptive mechanism for the different types of mixed pixels. Even for the boundary features in data 1, gains of 4.77% and 0.47% for the adjusted OA over BP and AM can be achieved. MASSM outperforms BP and AM, not only for the linear subpixel features but also for the boundary features. For data 3, with both features, the adjusted AD gives an improvement over BP and AM of 0.098 and 0.025. Generally speaking, the adjusted indices can reveal more distinct differences than the original ones. In addition, only allocation disagreement exists in the subpixel mapping results as the fraction images were simulated and are thought to be accurate. According to the statistical accuracy, the MASSM method exhibits the best overall classification accuracy for both features, when compared with the other two methods.

In addition to the classification accuracy, Table III provides a pairwise comparison of the four algorithms using the McNemar's test. The McNemar's test is a useful tool for determining whether two classification methods have significantly different prediction rates. From Table III, it can be seen that all the values of the McNemar's test are greater than the critical value (3.841459). This implies that all the classification methods have significantly different prediction rates, and MASSM is significantly more accurate than BP and AM. It is worth noting that the value of the McNemar's test between MASSM and AM for the artificial data 1 is the lowest (10.32). Although the value is still well above 3.841459, to some extent, it indicates that MASSM and AM both have the ability to map the boundary pixels.

B. Experiment 2—TM Remotely Sensed Image

subpixel mapping of remotely sensed images is a more complex problem as more land-cover classes may be contained in the mixed pixels. To better verify the performance of the proposed algorithm in a real environment, two remotely sensed images are used.

The proposed algorithm is tested with a 30-m resolution multispectral Landsat TM image from the three Gorges, China,

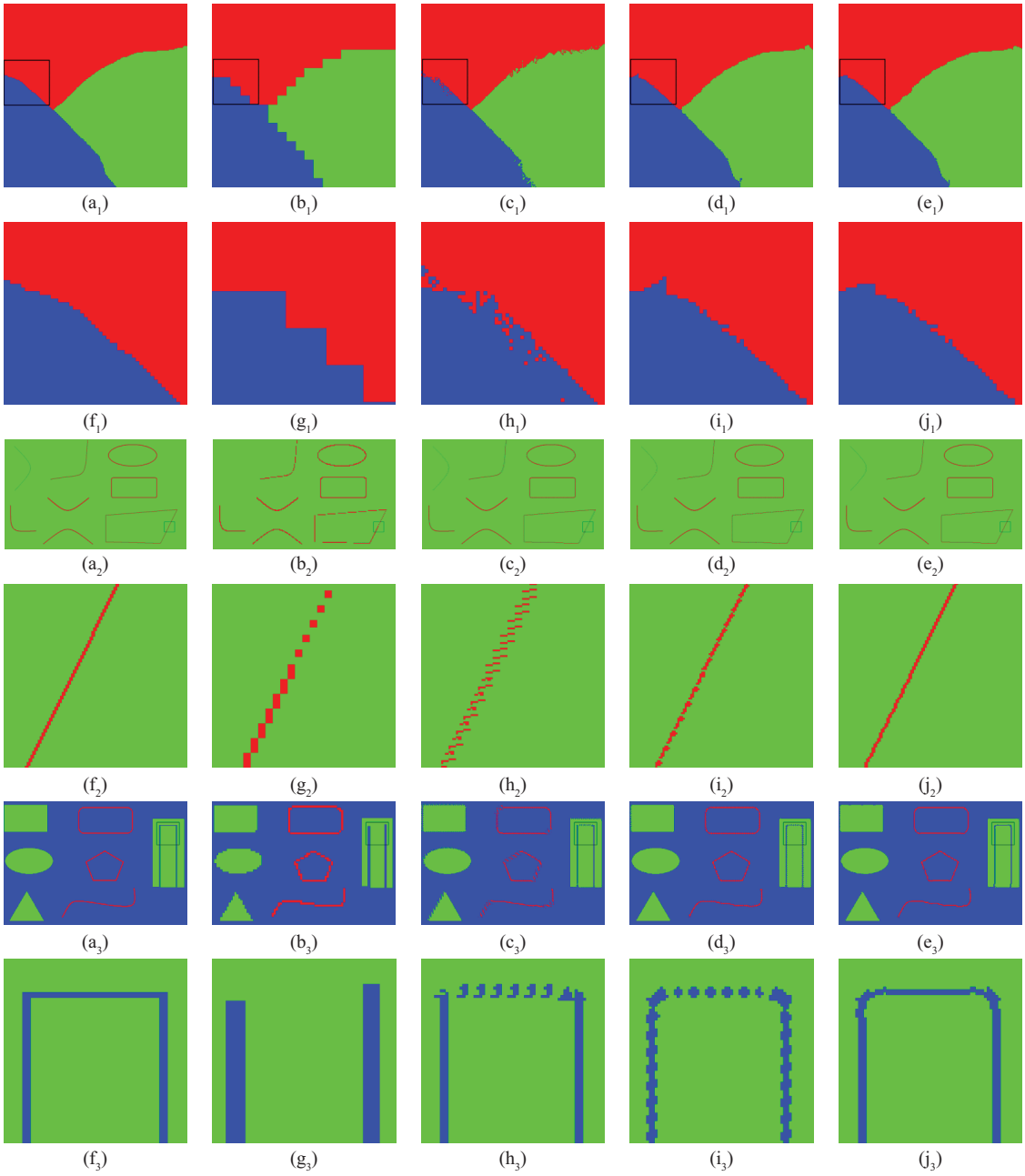

Fig. 11. subpixel mapping results for three artificial images with different methods. (a) Reference classification image. (b) Result of hard classification. (c) Result of the BP neural network. (d) Result of the attraction model (AC). (e) Result of the MASSM method. (f) Partial enlarged view of (a). (g) Partial enlarged view of (b). (h) Partial enlarged view of (c). (i) Partial enlarged view of (d). (j) Partial enlarged view of (e).

as shown in Fig. 12. The size of the TM image is 280 × 160. To form linear subpixels, the resize factor is set to 8. Three classes can be distinguished in this image.

To estimate the error introduced by the classification method, many pixels were manually selected as the ground truth, as Fig. 12(b) illustrates. In this paper, the reference classification map was obtained by classifying the original remotely sensed image with SVM, and the accuracy of SVM is shown in Table IV. As this image was not so complex, so that the distinct differences between classes can be observed, along with the impact of the selection of ground truth, SVM can be seen to be highly accurate, and the result was thought to be suitable for the experiments with subpixel mapping.

The most important feature in Fig. 12(a) is the river, which belongs to a linear feature. With the BP and AM methods, the river cannot be reconstructed well. However, the MASSM method can apparently obtain a better result than the previous methods. As Fig. 12 illustrates, the river in the MASSM result is continuous and complete, while that of the AM result has apparent holes in it, and the BP result is badly fractured.

The accuracies listed in Table V indicate the effectiveness of the proposed method. Compared with the previous artificial image 1, which contains only boundary features, this test

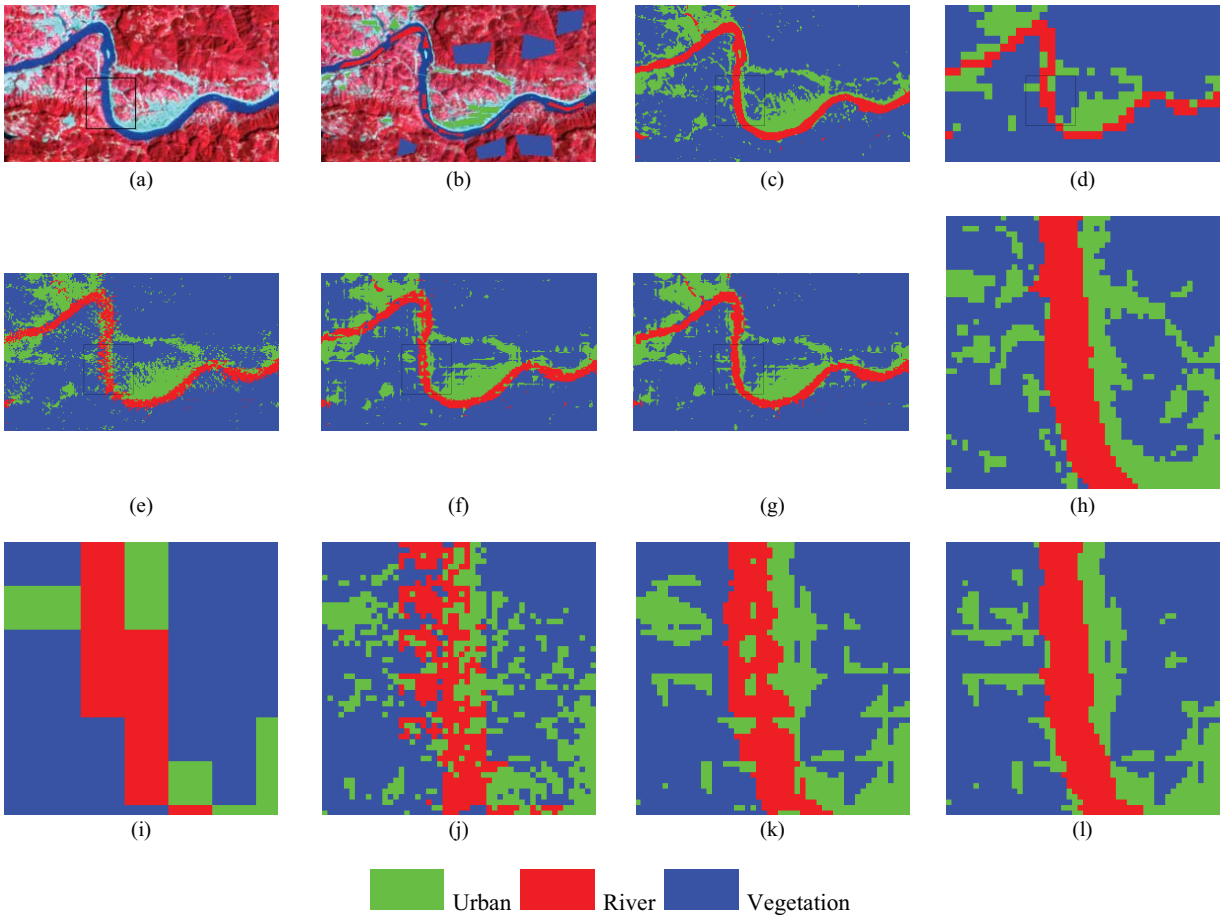

Fig. 12. subpixel mapping results for the synthetic TM remotely sensed image. (a) Original false color image. (b) Ground truth selected manually to evaluate the classification result. (c) Reference classification image obtained with SVM. (d) Result of hard classification. (e) BP neural network. (f) Attraction model. (g) MASSM. (h) Partial enlarged view of (c). (i) Partial enlarged view of (d). (j) Partial enlarged view of (e). (k) Partial enlarged view of (f). (l) Partial enlarged view of (g).

image is more challenging. The adjusted AD decreases from 0.198 and 0.196 for the BP and AM methods, respectively, to 0.186 for the proposed MASSM. The McNemar's test in Table VI demonstrates that MASSM gives significantly different results than the other subpixel mapping methods, compared to the critical value (3.841459). The TM image is less complex, and pure pixels occupy quite a few proportions, especially for the vegetation. As the river does not occupy the main part of the image, and the boundary features are not so apparent, because of the large resize factor, the gain in accuracy is far below that of the artificial images. The confusion matrix in Table VII reveals that the MASSM method has a better result than BP and AM on the river, and the greatest confusion is between urban and vegetation because they are the main land-cover classes in this image and intersect with each other. However, both the visual assessment and accuracies still indicate that MASSM is an effective method in mapping the different structures in mixed pixels, compared with BP and AM.

C. Experiment 3—QuickBird Remotely Sensed Image

In this section, a multispectral QuickBird (March 2004; 2.4 m resolution) dataset is classified with eCognition software to preserve the internal consistency of classes. The size of the QuickBird data is 180 × 180. The classification map is then degraded to obtain a simulated fraction image with a resize factor of 6, which is greater than the widths of most of the linear features in this dataset. The three subpixel mapping methods and HC are then used, and the results are shown in Fig. 13.

Unlike the TM image, the QuickBird image was classified by eCognition software to overcome the spectral diversity of the same classes, such as the house class. The classification accuracy is illustrated in Table VIII. This result shows that misclassification happens between road and vegetation, due to the geographic proximity. Similarly, it also occurs between house and bare soil.

These kinds of misclassification may occur in the following subpixel mapping experiments. However, this classification map can be used as a reference image for subpixel mapping, with an OA of 93.92%.

The visual comparison of the three results suggests that the MASSM method is superior to the other three methods. Fractured lines can be clearly found in the results of BP and AM. For the HC method, although the straight road in the left of Fig. 13(c) looks acceptable, the quantity information has been lost. The AM method obtains an acceptable result

TABLE II
ACCURACY OF SUBPIXEL MAPPING WITH THE ARTIFICIAL DATA

Accuracy		HC	BP	AM	MASSM
Artificial data 1	QD	0.002	0	0	0
	AD	0.017	0.008	0.004	0.003
	OA	98.87%	99.21%	99.63%	99.67%
	adjusted QD	0.022	0	0	0
	adjusted AD	0.171	0.082	0.038	0.034
	adjusted OA	80.67%	91.85%	96.15%	96.62%
Artificial data 2	QD	0.008	0	0	0
	AD	0.006	0.007	0.006	0.005
	OA	98.63%	99.27%	99.44%	99.54%
	adjusted QD	0.187	0	0	0
	adjusted AD	0.138	0.173	0.132	0.108
	adjusted OA	67.51%	82.74%	86.80%	89.17%
Artificial data 3	QD	0.016	0	0	0
	AD	0.024	0.020	0.012	0.010
	OA	95.97%	98.02%	98.71%	99.01%
	adjusted QD	0.156	0	0	0
	adjusted AD	0.210	0.194	0.121	0.096
	adjusted OA	63.42%	80.65%	87.40%	90.44%

TABLE III
MCNEMAR'S TEST WITH THE ARTIFICIAL DATASETS

Datasets	Methods	HC	BP	AM	MASSM
Artificial data 1	HC	–	250.30	487.41	516.95
	BP		–	76.20	96.14
	AM			–	10.32
	MASSM				–
Artificial data 2	HC	–	1467.54	2353.48	2928.58
	BP		–	201.71	468.17
	AM			–	89.87
	MASSM				–
Artificial data 3	HC	–	2032.52	3767.77	4495.80
	BP		–	560.42	1088.33
	AM			–	168.48
	MASSM				–

TABLE IV
ACCURACY OF THE CLASSIFICATION METHODS FOR THE TM IMAGE

Methods	Class	River	Urban	Vegetation
SVM	River	811	0	0
	Urban	1	961	4
	Vegetation	0	3	3410
OA = 99.85%				

TABLE V
ACCURACY OF SUBPIXEL MAPPING WITH THE TM IMAGE

Accuracy		HC	BP	AM	MASSM
TM Image	QD	0.03	0	0	0
	AD	0.10	0.115	0.114	0.108
	OA	87.60%	88.51%	88.63%	89.22%
	adjusted QD	0.05	0	0	0
	adjusted AD	0.167	0.198	0.196	0.186
	adjusted OA	78.61%	80.18%	80.40%	81.42%

TABLE VI
MCNEMAR'S TEST WITH THE TM IMAGE

Dataset	Methods	HC	BP	AM	MASSM
TM image	HC	–	31.20	40.74	129.45
	BP		–	0.60	30.40
	AM			–	49.64
	MASSM				–

TABLE VII
CONFUSION MATRIX FOR THE TM IMAGE

Methods	Class	River	Urban	Vegetation
HC	River	2758	681	593
	Urban	337	4877	1378
	Vegetation	326	2242	31 608
BP	River	2673	437	311
	Urban	454	5528	1818
	Vegetation	294	1835	31 450
AM	River	2901	300	220
	Urban	390	5429	1981
	Vegetation	130	2071	31 378
MASSM	River	3036	214	138
	Urban	238	5332	1760
	Vegetation	147	2254	31 681

on boundary features, while linear subpixel features cannot be reconstructed well as they are thought to be boundary features, and the corresponding algorithm destroys the continuity of lines. The BP method performs worse than AM and MASSM, for both linear features and boundary features. The MASSM method works well with most roads, except some sections where the environment is too complex. Some of the enlarged views demonstrate that the MASSM method is better than the BP and AM methods, as Fig. 13(g)–(k) illustrates.

Table IX shows the accuracy of the QuickBird image for the different methods. The results verify the judgment of the visual assessment that the MASSM method is superior to the BP and AM methods. All the subpixel mapping results have a higher accuracy than the HC. An improvement of 0.059 and 0.017 for the adjusted AD is obtained by the MASSM method, compared with BP and AM, respectively, when the McNemar's value is compared to a critical value, as shown in Table X. This indicates that MASSM gives a significantly different performance, compared to the other methods, as discussed in this experiment.

There are four classes in the QuickBird image, and the situation of mixed pixels is more complex than with the artificial images. Most roads belong to linear features, and other classes are thought to be boundary features. The confusion matrix in Table XI shows that the MASSM method produces better results than the other methods for the road class. The house class was mainly confused with vegetation because of the geographic proximity. Although the results of the house class with the MASSM method are a little inferior to AM, the other two classes have a higher precision than BP and AM. However, MASSM outperforms the other methods in mapping the different features in mixed pixels, in both visual assessment and accuracy.

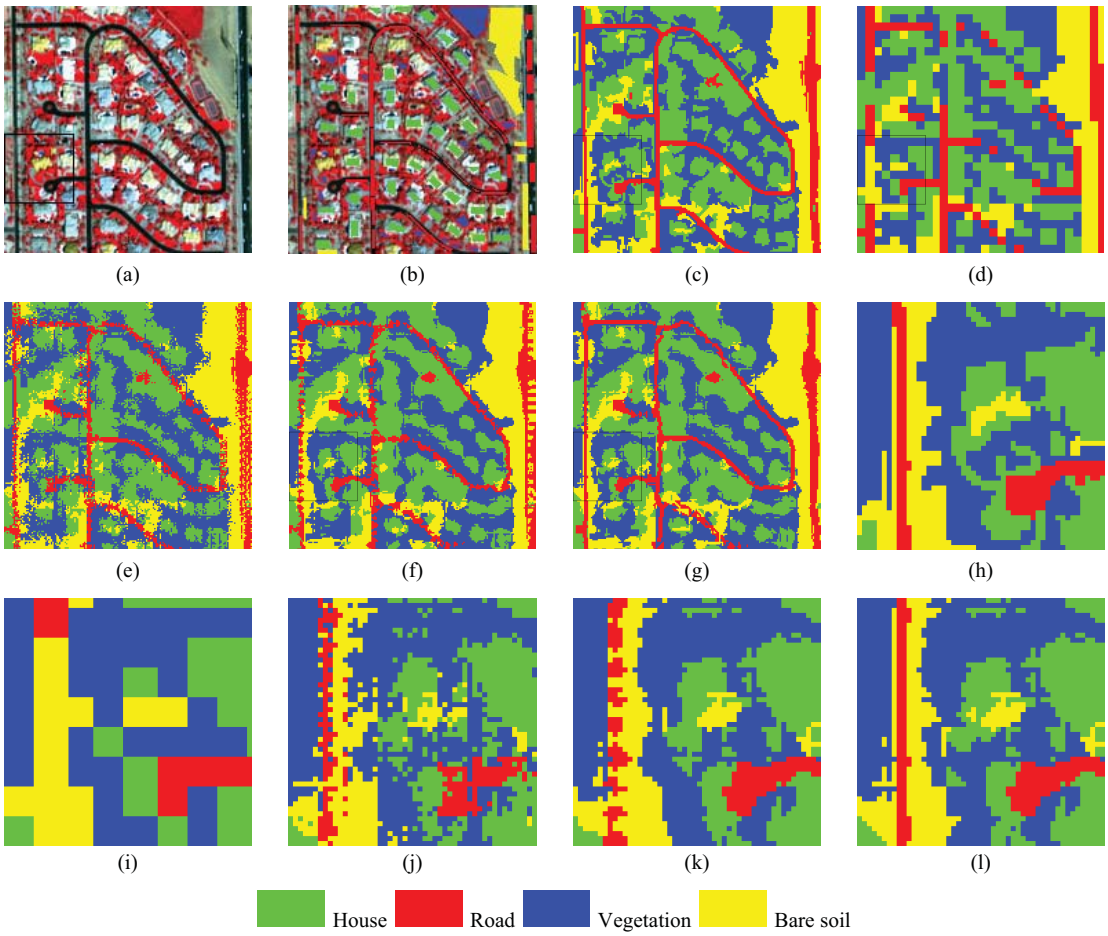

Fig. 13. subpixel mapping results for the QuickBird remotely sensed image. (a) Original false color image. (b) Ground truth selected manually to evaluate the classification result. (c) Reference classification image. (d) Result of hard classification. (e) BP neural network. (f) Attraction model. (g) MASSM. (h) Partial enlarged view of (c). (i) Partial enlarged view of (d). (j) Partial enlarged view of (e). (k) Partial enlarged view of (f). (l) Partial enlarged view of (g).

TABLE VIII
ACCURACY OF THE CLASSIFICATION METHODS WITH THE QUICKBIRD IMAGE

Methods	Class	Road	House	Vegetation	Bare Soil
eCognition	Road	1219	34	0	6
	House	11	1618	0	0
	Vegetation	106	38	722	3
	Bare soil	5	128	2	1585
OA = 93.92%					

TABLE IX
ACCURACY OF SUBPIXEL MAPPING WITH THE QUICKBIRD IMAGE

Accuracy		HC	BP	AM	MASSM
QuickBird Image	QD	0.025	0	0	0
	AD	0.226	0.206	0.174	0.160
	OA	74.91%	79.36%	82.57%	83.94%
	adjusted QD	0.032	0	0	0
	adjusted AD	0.285	0.265	0.223	0.206
	adjusted OA	67.83%	73.54%	77.66%	79.42%

TABLE X
MCNEMAR'S TEST WITH THE QUICKBIRD IMAGE

Dataset	Methods	HC	BP	AM	MASSM
QuickBird Image	HC	–	265.74	810.04	1115.90
	BP		–	177.17	348.33
	AM			–	77.55
	MASSM				–

D. Parameter Analysis

Parameters are important to the MASSM method, and when it comes to subpixel mapping, two different types of parameters are considered. One is the resize factor S, which is relevant to the subpixel mapping itself, and the other type are parameters belonging to MASSM, which include the agent number N and the agent life T. As the interaction between N and T is so strong, they should be considered carefully. The impacts of some other procedures are also discussed.

1) Impact of the Resize Factor S: In this analysis, test 3 of the artificial images in Fig. 10 and the QuickBird image in Fig. 13 are used. Fig. 14 illustrates the impact of S for both images. Generally speaking, the accuracy decreases as S increases. This is because, as S increases, the internal structure of a mixed pixel will be too complex to interpret and hard to reconstruct. The spatial dependence assumption does not work when S is too large. For the artificial image, the adjusted OA

TABLE XI
CONFUSION MATRIX FOR THE QUICKBIRD IMAGE

Methods	Class	Road	House	Vegetation	Bare Soil
HC	Road	2606	543	722	719
	House	236	8175	1680	505
	Vegetation	378	1603	8609	522
	Bare soil	571	260	391	4880
BP	Road	2724	255	394	418
	House	228	8617	1383	353
	Vegetation	415	1351	9076	560
	Bare soil	424	358	549	5295
AM	Road	2768	211	382	430
	House	190	8944	1122	325
	Vegetation	407	1107	9529	359
	Bare soil	426	319	369	5512
MASSM	Road	3042	236	313	200
	House	212	8881	1155	333
	Vegetation	334	1136	9557	375
	Bare soil	203	328	377	5718

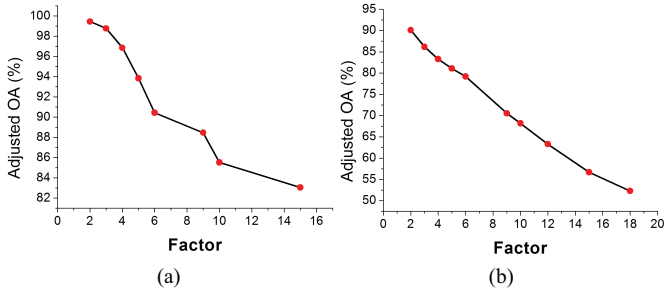

Fig. 14. (a) Impact of S for the artificial image. (b) Impact of S for the remotely sensed image.

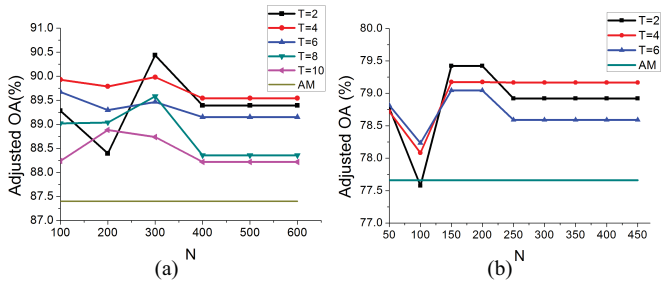

Fig. 15. (a) Impact of different N and T for the artificial image. (b) Impact of different N and T for the remotely sensed image.

is still acceptable, even when S is 18, because the shapes of classes are simple and regular. However, the accuracy of the QuickBird image appears to decrease as S increases. The adjusted OA is less than 0.6 when S is more than 8. It is therefore impossible to enhance the resolution infinitely. The choice of suitable resize factor is important in subpixel mapping.

2) Impact of Agent Number N and Agent Life T: In this analysis, test 3 of the artificial images in Fig. 10 and the QuickBird image in Fig. 13 are used. The resize factor S is 6 for both the artificial image and the QuickBird image. Fig. 15 depicts the impact of different N and T on the accuracy. As the selection of one parameter has an impact on the other,

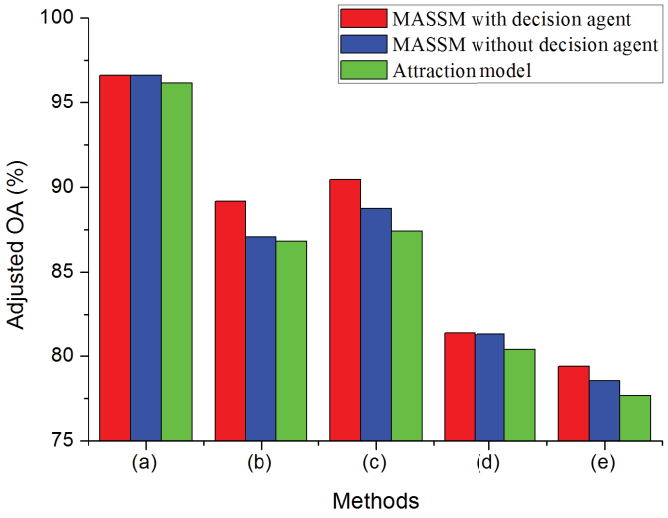

Fig. 16. Impact of the decision agent with different datasets. (a) Artificial image 1. (b) Artificial image 2. (c) Artificial image 3. (d) Remotely sensed image 1—TM. (e) Remotely sensed image 2—QuickBird.

different combinations of N and T are tested. It can be seen that the accuracy differs for the different combinations. The precision with different combinations of N and T is compared to each other and that of the AC. The curves of different T are similar to each other, and the optimal N for every T may be the same. Generally speaking, the agent number N should be set at a higher level to detect different structures in images, and the life T should be set at a lower level to avoid confusion between different features. There are, though, still some combinations that do not fulfill the previous assumption. However, Fig. 15 reveals that the accuracy of most combinations is higher than that of the AM method. It may be difficult to obtain the highest accuracy when applying MASSM; however, MASSM outperforms the AM method in most cases.

3) Impact of the Decision Agent: In the proposed method, a decision agent is an essential component for coordinating the contradictions of other agents, such as the feature detection agent and subpixel mapping agent, to obtain a global solution. However, the effectiveness of the decision agent in improving the accuracy of subpixel mapping still needs to be verified. In this experiment, three artificial images and two remotely sensed images are used to test the impact of the decision agent on the proposed method. As Fig. 16 illustrates, no matter which decision agent is used, the proposed method performs better than the traditional AC. However, when the decision agent is utilized, the accuracy of the proposed method can be improved for most datasets, except artificial image 1. This is because artificial image 1 contains only boundary features, and few contradictions exist to invoke the decision agent. Generally speaking, the decision agent can improve the accuracy of subpixel mapping, and it is an essential component of the proposed method.

4) Impact of the Initialization of the Feature Detection Agents: Generally speaking, there are two kinds of initialization of the FDAs. One approach is to spread the agents equally on the image, and the other is to spread them randomly. In this paper, we adopt the former strategy. To confirm the reliability

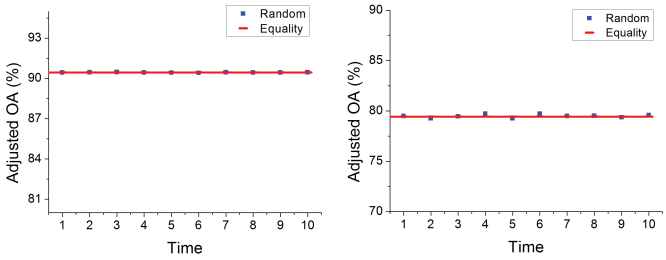

Fig. 17. Impact of the initialization of the feature detection agents. (a) Artificial image 3. (b) Remotely sensed image 2—QuickBird.

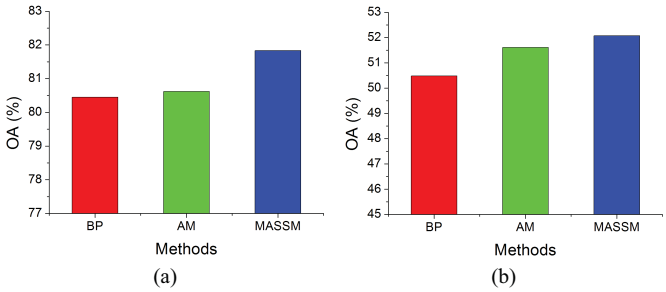

Fig. 18. Accuracy of the different subpixel mapping methods for this special procedure. (a) Remotely sensed image 1—TM. (b) Remotely sensed image 2—QuickBird.

of the proposed method, we undertook some experiments regarding the initial placement of the FDAs. Artificial image 3 and remotely sensed image 2 were experimented with, and the proposed method with a random strategy of FDAs was executed 10 times. As Fig. 17 illustrates, the initial placement of FDAs has little impact on the accuracy of the proposed method. For both images, the accuracy with a random strategy fluctuates around the accuracy of the equality strategy. In other words, the two strategies are both suitable for the proposed method.

5) Impact of the Procedure of the Experiments: In this experiment, two remotely sensed images are used. In this procedure, the steps are: 1) resample the original high-resolution image to the coarser scale, using a point-spread function in which the size is 3×3 and the variance is 0.4, adding Gaussian noise in which the variance is 5; 2) The fully constrained least squares method is applied to obtain the fraction image at the coarse resolution; 3) BP, the AC and the proposed method are applied to the fraction image generated at 2); and 4) Classification of the original high-resolution image is used to test the accuracy of the different subpixel mapping methods. For the TM image, the resize factor is 8, and for the QuickBird image it is 6. As Fig. 18 illustrates, due to the errors introduced by the spectral unmixing and classification, the accuracies of the subpixel mapping methods implemented on the results of the spectral unmixing are decreased greatly when compared with those based on a fraction image derived from the classification map. However, the experiments reveal that the proposed method can obtain a higher accuracy than the other two subpixel mapping methods when conducted on a fraction image that was generated by the spectral unmixing of a coarse image.

V. Conclusion

In this paper, a novel subpixel mapping framework based on an MAS, namely MASSM, was proposed to adaptively deal with the different types of mixed pixels. Most traditional subpixel mapping methods focus on how to maximize the spatial dependence, while ignoring the inherent structures in mixed pixels, such as a linear subpixel, which may not be effectively reconstructed by this kind of approach. To avoid the problem, three kinds of agents, FDAs, SMAs and DAs, are designed to tackle the problem of subpixel mapping in the proposed MASSM algorithm to better reconstruct the different types of mixed pixels.

In MASSM, FDAs are first created to determine the types of mixed pixels by calculating the MLI. By use of the FDAs, the pixels can be classified into three kinds of pixels: pure pixel, boundary-mixed pixel and linear subpixel. The different types of pixels then have the corresponding SMAs applied, which are used to finish the task of the subpixel mapping. In particular, a novel subpixel mapping method for linear subpixel features is proposed by extracting the center line. Lastly, DAs are used to coordinate any contradiction that occurs during the implementation of FDAs and SMAs, to obtain the optimal subpixel mapping result.

In the experiments using different images (three synthetic artificial images and two synthetic remote-sensing images), compared with the traditional subpixel mapping methods (the BP subpixel mapping algorithm and the spatial attraction subpixel mapping model), MASSM was able to achieve better results with a higher subpixel mapping accuracy. This confirms that MASSM is appropriate for the subpixel mapping of remote-sensing images. Our future work will focus on further improvements to the proposed technique, such as the adaptive selection of parameters.

Acknowledgment

The authors would like to thank the editor, associate editor, and the anonymous reviewers for helpful comments and suggestions, and also Beijing Panorama Space Technology Corporation Limited, Beijing, China, for providing the free QuickBird image.

References

[1] G. G. Wilkinson, "Results and implications of a study of fifteen years of satellite image classification experiments," *IEEE Trans. Geosci. Remote Sens.*, vol. 43, no. 3, pp. 433–440, Mar. 2005.

[2] G. M. Foody, "Hard and soft classifications by a neural network with a non-exhaustively defined set of classes," *Int. J. Remote Sens.*, vol. 23, no. 18, pp. 3853–3864, Jan. 2002.

[3] X. Ceamanos, S. Douté, B. Luo, F. Schmidt, G. Jouannic, and J. Chanussot, "Intercomparison and validation of techniques for spectral unmixing of hyperspectral images: A planetary case study," *IEEE Trans. Geosci. Remote Sens.*, vol. 49, no. 11, pp. 4341–4358, Nov. 2011.

[4] R. Heylen, D. Burazerovic, and P. Scheunders, "Fully constrained least squares spectral unmixing by simplex projection," *IEEE Trans. Geosci. Remote Sens.*, vol. 49, no. 11, pp. 4112–4122, Nov. 2011.

[5] M.-D. Iordache, J. Bioucas-Dias, and A. Plaza, "Sparse unmixing of hyperspectral data," *IEEE Trans. Geosci. Remote Sens.*, vol. 49, no. 6, pp. 2014–2039, Jun. 2011.

[6] P. M. Atkinson, "Mapping sub-pixel boundaries from remotely sensed images," *Innovations in GIS IV*. London, U.K.: Taylor & Francis, 1997, ch. 12, pp. 166–180.

[7] J. Gavin and C. Jennison, "A subpixel image restoration algorithm," *J. Comput. Graph. Stat.*, vol. 6, no. 2, pp. 182–201, Jun. 1997.

[8] P. M. Atkinson, "Issues of uncertainty in super-resolution mapping and the design of an inter-comparison study," in *Proc. 8th Int. Symp. Spatial Accur. Assessm. Natural Res. Envir. Sci.*, Shanghai, China, 2004, pp. 145–154.

[9] A. Boucher and P. C. Kyriakidis, "Super-resolution land cover mapping with indicator geostatistics," *Remote Sens. Environ.*, vol. 104, no. 3, pp. 264–282, Oct. 2006.

[10] A. Boucher, P. C. Kyriakidis, and C. Cronkite-Ratcliff, "Geostatistical solutions for super-resolution land cover mapping," *IEEE Trans. Geosci. Remote Sens.*, vol. 46, no. 1, pp. 272–283, Jan. 2008.

[11] A. Boucher and P. C. Kyriakidis, "Integrating fine scale information in super-resolution land-cover mapping," *Photogramm. Eng. Remote Sens.*, vol. 73, no. 8, pp. 913–921, 2007.

[12] J. Verhoeye and R. D. Wulf, "Land cover mapping at sub-pixel scales using linear optimization techniques," *Remote Sens. Environ.*, vol. 79, no. 1, pp. 96–104, Jan. 2002.

[13] K. C. Mertens, L. P. C. Verbeke, and R. R. D. Wulf, "Sub-pixel mapping with neural networks: Real-world spatial configurations learned from artificial shapes," in *Proc. 4th Int. Symp. Remote Sens.*, Jun. 2003, pp. 1–5.

[14] K. C. Mertens, L. P. C. Verbeke, T. Westra, and R. R. D. Wulf, "Sub-pixel mapping and sub-pixel sharpening using neural network predicted wavelet coefficients," *Remote Sens. Environ.*, vol. 91, no. 2, pp. 225–236, May 2004.

[15] L. Zhang, K. Wu, Y. Zhong, and P. Li, "A new sub-pixel mapping algorithm based on a BP neural network with an observation model," *Neurocomputing*, vol. 71, nos. 10–12, pp. 2046–2054, Jun. 2008.

[16] P. M. Atkinson, "Sub-pixel target mapping from soft-classified, remotely sensed imagery," *Photogramm. Eng. Remote Sens.*, vol. 71, no. 7, pp. 839–846, Jul. 2005.

[17] M. W. Thornton, P. M. Atkinson, and D. A. Holland, "A linearised pixel-swapping method for mapping rural linear land cover features from fine spatial resolution remotely sensed imagery," *Comput. Geosci.*, vol. 33, no. 10, pp. 1261–1272, Oct. 2007.

[18] M. W. Thornton, P. M. Atkinson, and D. A. Holland, "Sub-pixel mapping of rural land cover objects from fine spatial resolution satellite sensor imagery using super-resolution pixel-swapping," *Int. J. Remote Sens.*, vol. 27, no. 3, pp. 473–491, Feb. 2006.

[19] A. J. Tatem, H. G. Lewis, P. M. Atkinson, and M. S. Nixon, "Super-resolution target identification from remotely sensed images using a Hopfield neural network," *IEEE Trans. Geosci. Remote Sens.*, vol. 39, no. 4, pp. 781–796, Apr. 2001.

[20] A. J. Tatem, H. G. Lewis, P. M. Atkinson, and M. S. Nixon, "Multiple-class land-cover mapping at the sub-pixel scale using a Hopfield neural network," *Int. J. Appl. Earth Obs. Geoinf.*, vol. 3, no. 2, pp. 184–190, 2001.

[21] A. J. Tatem, H. G. Lewis, P. M. Atkinson, and M. S. Nixon, "Super-resolution land cover pattern prediction using a Hopfield neural network," *Remote Sens. Environ.*, vol. 79, no. 1, pp. 1–14, Jan. 2002.

[22] K. C. Mertens, L. P. C. Verbeke, E. I. Ducheyne, and R. R. D. Wulf, "Using genetic algorithms in sub-pixel mapping," *Int. J. Remote Sens.*, vol. 24, no. 21, pp. 4241–4247, Nov. 2003.

[23] Y. Zhong and L. Zhang, "Remote sensing image sub-pixel mapping based on adaptive differential evolution," *IEEE Trans. Syst. Man, Cybern. B, Cybern.*, vol. 42, no. 5, pp. 1306–1329, Oct. 2012.

[24] K. C. Mertens, B. D. Baets, L. P. C. Verbeke, and R. R. D. Wulf, "A sub-pixel mapping algorithm based on sub-pixel/pixel spatial attraction models," *Int. J. Remote Sens.*, vol. 27, no. 15, pp. 3293–3310, Aug. 2006.

[25] T. Kasetkasem, M. K. Arora, and P. K. Varshney, "Super-resolution land cover mapping using a markov random field based approach," *Remote Sens. Environ.*, vol. 96, nos. 3–4, pp. 302–314, Jun. 2005.

[26] V. A. Tolpekin and A. Stein, "Quantification of the effects of land-cover-class spectral separability on the accuracy of markov-random-field-based superresolution mapping," *IEEE Trans. Geosci. Remote Sens.*, vol. 47, no. 9, pp. 3283–3297, Sep. 2009.

[27] L. Wang and Q. Wang, "Subpixel mapping using Markov random field with multiple spectral constraints from subpixel shifted remote sensing images," *IEEE Geosci. Remote Sens. Lett.*, vol. 10, no. 3, pp. 598–602, May 2013.

[28] Y. Ge, S. Li, and V. C. Lakhan, "Development and testing of a subpixel mapping algorithm," *IEEE Trans. Geosci. Remote Sens.*, vol. 47, no. 7, pp. 2155–2164, Jul. 2009.

[29] P. Fisher, "The pixel: A snare and a delusion," *Int. J. Remote Sens.*, vol. 18, no. 3, pp. 679–685, Feb. 1997.

[30] K. S. Ettabaa, I. R. Farah, and M. B. Ahmed, "Multiagent system for detecting and analysing changes on satellite image sequence," in *Proc. IEEE Int. Conf. Ind. Technol.*, Dec. 2004, pp. 1579–1584.

[31] M. Chitsaz and S. Woo Chaw, "A multiagent system approach for medical image segmentation," in *Proc. Int. Conf. Future Comput. Commun.*, Apr. 2009, pp. 408–411.

[32] J. M. Liu and Y. Y. Tang, "Adaptive image segmentation with distributed behavior-based agents," *IEEE Trans. Pattern Anal. Mach. Intell.*, vol. 21, no. 6, pp. 544–551, Jun. 1999.

[33] B. Wei, L. Zhang, and P. Li, "A method for image segmentation based on random diffused agents," *J. Image Graph.*, vol. 12, no. 12, pp. 2113–2118, Dec. 2007.

[34] N. V. Findler and R. Lo, "An examination of distributed planning in the world of air traffic control," *J. Parallel Distr. Com.*, vol. 3, no. 3, pp. 411–431, Sep. 1986.

[35] R. Steeb, S. J. Cammarata, F. A. Hayes-Roth, P. W. Thorndyke, and R. Wesson, "Distributed intelligence for air fleet control," Rep. R-2728-ARPA, Dept. Comput. Sci., Univ. Stanford, Stanford, CA, USA, 1981.

[36] C. Guilfoyle, J. Jeffcoate, and H. Stark, *Agents on the WEB: Catalyst for E-Commerce*. London, U.K.: Ovum Ltd. Apr. 1997.

[37] C. Guilfoyle and E. Warner, *Intelligent Agents: The New Revolution in Software*. London, U.K.: Ovum Ltd. May 1994.

[38] T. E. Downing, S. Moss, and C. P. Wostl, "Understanding climate policy using participatory agent-based social simulation," *Multiagent Based Simul.*, 2001, pp. 127–140.

[39] W. R. Tobler, "A computer movie simulating urban growth in the Detroit region," *Econom. Geograph.*, vol. 46, pp. 234–240, Jun. 1970.

[40] D. Song and D. Tao, "Biologically inspired feature manifold for scene classification," *IEEE Trans. Image Process.*, vol. 19, no. 1, pp. 174–184, Jan. 2010.

[41] K. Huang, D. Tao, Y. Yuan, X. Li, and T. Tan, "Biologically inspired features for scene classification in video surveillance," *IEEE Trans. Syst. Man, Cybern. Part B, Cybern.*, vol. 41, no. 1, pp. 307–313, Feb. 2011.

[42] A. M. Muad, "Super resolution mapping," Ph.D. dissertation, School Geography, Univ. Nottingham, U.K., 2011.

[43] A. M. Muad and G. M. Foody, "Super-resolution mapping of lakes from imagery with a coarse spatial and fine temporal resolution," *Int. J. Appl. Earth Observ. Geoinf.*, vol. 15, pp. 79–91, Apr. 2012.

[44] A. M. Muad and G. M. Foody, "Impact of land cover patch size on the accuracy of patch area representation in HNN-based super resolution mapping," *IEEE J. Sel. Topics Appl. Earth Observ. Remote Sens.*, vol. 5, no. 5, pp. 1418–1427, Oct. 2012.

[45] M. Wooldridge, *An Introduction to Multiagent Systems*. New York, USA: Wiley, 2002.

[46] M. Wooldridge, "Agent-based software engineering," *IEEE Trans. Softw. Eng.*, vol. 144, no. 1, pp. 26–37, Feb. 1997.

[47] M. Wooldridge and N. R. Jennings, "Intelligent agents: Theory and practice," *Knowl. Eng. Rev.*, vol. 10, no. 2, pp. 115–152, Jun. 1995.

[48] E. G. P. Bovenkamp, J. Dijkstra, J. G. Bosch, and J. H. C. Reiber, "User-agent cooperation in multiagent IVUS image segmentation," *IEEE Trans. Med. Imag.*, vol. 28, no. 1, pp. 94–105, Jan. 2009.

[49] J. M. Liu, Y. Y. Tang, and Y. C. Cao, "An evolutionary autonomous agents approach to image feature extraction," *IEEE Trans. Evol. Comput.*, vol. 1, no. 2, pp. 141–158, Jul. 1997.

[50] N. R. Jennings, "On agent-based software engineering," *Artif. Intell. J.*, vol. 117, no. 2, pp. 277–296, Mar. 2000.

[51] T. Zhou, D. Tao, and X. Wu, "Manifold elastic net: A unified framework for sparse dimension reduction," *Data Mining Knowl. Discov.*, vol. 22, no. 3, pp. 340–371, May 2011.

[52] W. Bian and D. Tao, "Max-min distance analysis by using sequential SDP relaxation for dimension reduction," *IEEE Trans. Pattern Anal. Mach. Intell.*, vol. 33, no. 5, pp. 1037–1050, May 2011.

[53] R. G. Pontius and M. Millone, "Death to kappa: Birth of quantity disagreement and allocation disagreement for accuracy assessment," *Int. J. Remote Sens.*, vol. 32, no. 15, pp. 4407–4429, Aug. 2011.

[54] Q. McNemar, "Note on the sampling error of the difference between correlated proportions or percentages," *Psychometrika*, vol. 12, no. 2, pp. 153–157, Jun. 1947.

[55] O. Debeir, I. Van den Steen, P. Latinne, P. Van Ham, and E. Wolff, "Textural and contextual land-cover classification using single and multiple classifier systems," *Photogramm. Eng. Remote Sens.*, vol. 68, no. 6, pp. 597–606, Jun. 2002.

[56] Y. Zhong and L. Zhang, "An adaptive artificial immune network for supervised classification of multi-/hyperspectral remote sensing imagery," *IEEE Trans. Geosci. Remote Sens.*, vol. 50, no. 3, pp. 894–909, Mar. 2012.

[57] E. Alpaydin, *Introduction to Machine Learning*. Cambridge, MA, USA: MIT Press, Oct. 2004.

Xiong Xu received the B.S. degree in photogrammetry from Wuhan University, Wuhan, China, in 2008, where he is currently pursuing the Ph.D. degree in photogrammetry and remote sensing with the State Key Laboratory of Information Engineering in Surveying, Mapping, and Remote Sensing.

His current research interests include multispectral and hyperspectral image processing, artificial neural networks, and pattern recognition.

Yanfei Zhong (M'11) received the B.S. degree in information engineering and the Ph.D. degree in photogrammetry and remote sensing from Wuhan University, Wuhan, China, in 2002 and 2007, respectively.

He has been with the State Key Laboratory of Information Engineering in Surveying, Mapping and Remote Sensing, Wuhan University, since 2007, and is currently a Professor. His current research interests include multi- and hyperspectral remote sensing image processing, artificial intelligence, and pattern recognition. He has authored more than 15 peer-reviewed articles in international journals, such as the IEEE TRANSACTIONS ON GEOSCIENCE AND REMOTE SENSING and the IEEE TRANSACTIONS ON SYSTEMS, MAN, AND CYBERNETICS PART B.

Dr. Zhong was the recipient of the National Excellent Doctoral Dissertation Award of China in 2009 and New Century Excellent Talents in University of China in 2009. He was a Referee of the IEEE TRANSACTIONS ON GEOSCIENCE AND REMOTE SENSING, the IEEE TRANSACTIONS ON SYSTEMS, MAN, AND CYBERNETICS PART B, the IEEE JOURNAL OF SELECTED TOPICS IN APPLIED EARTH OBSERVATIONS AND REMOTE SENSING, and *Pattern Recognition*.

Liangpei Zhang (M'06–SM'08) received the B.S. degree in physics from Hunan Normal University, Changsha, China, in 1982, the M.S. degree in optics from the Xi'an Institute of Optics and Precision Mechanics of the Chinese Academy of Sciences, Xi'an, China, in 1988, and the Ph.D. degree in photogrammetry and remote sensing from Wuhan University, Wuhan, China, in 1998.

He is currently with the State Key Laboratory of Information Engineering in Surveying, Mapping and Remote Sensing, Wuhan University, as the Head of the Remote Sensing Division. He is also a "Chang-Jiang Scholar" Chair Professor appointed by the Ministry of Education, China. He is currently the Principal Scientist for the China State Key Basic Research Project (2011–2016) appointed by the Ministry of National Science and Technology of China to lead the remote sensing program in China. He has authored more than 260 research papers and holds five patents. His current research interests include hyperspectral remote sensing, high resolution remote sensing, image processing, and artificial intelligence.

Dr. Zhang is a Fellow of the Institution of Electrical Engineers, an Executive Member for the China Society of Image and Graphics, and others. He is an Executive Member (Board of Governors) of the China National Committee of the International Geosphere-Biosphere Programme. He regularly serves as a Co-Chair of the series SPIE Conferences on Multispectral Image Processing and Pattern Recognition, Conference on Asia Remote Sensing, and many other conferences. He edits several conference proceedings, issues, and the Geoinformatics Symposiums. He also serves as an Associate Editor of the *International Journal of Ambient Computing and Intelligence,* the *International Journal of Image and Graphics*, the *International Journal of Digital Multimedia Broadcasting*, the *Journal of Geo-spatial Information Science*, and the *Journal of Remote Sensing*. He is currently serving as an Associate Editor for the IEEE TRANSACTIONS ON GEOSCIENCE AND REMOTE SENSING.